Journal of Marine Systems xxx (2009) xxx–xxx

Contents lists available at ScienceDirect

Journal of Marine Systems

journal homepage: www.elsevier.com/locate/jmarsys

Modeling the effect of ENSO on the lower trophic level ecosystem of the Cold Tongue and the Warm Pool regions in the equatorial Pacific

B. Salihoglu *

Center for Coastal Physical Oceanography, ODU, Norfolk, VA, United States
LEGOS/CNRS, Toulouse, France
Institute of Marine Sciences, Middle East Technical University, Erdemli, Turkey

ARTICLE INFO

Article history:
Received 18 January 2007
Received in revised form 18 December 2008
Accepted 23 December 2008
Available online xxxx

Keywords:
Equatorial Pacific
Ecosystem modeling
ENSO
Carbon cycle
Iron
Phytoplankton

ABSTRACT

The effects of El Niño-Southern Oscillation (ENSO) processes on the lower trophic levels of Cold Tongue (140°W) region were examined with eight-year simulations for a time, 1991–1999, that included three ENSO cycles. As a comparison, simulations were done for a region in the western Pacific at 165°E at the equator, which is known as the Warm Pool. A one-dimensional multi-component lower trophic level ecosystem model that includes detailed algal physiology is used, which is forced by an eight-year time series of spectrally-dependent light, temperature, and water column mixing obtained from a Tropical Atmosphere-Ocean (TAO) Array mooring. Autotrophic growth is represented by five algal groups, which have light and nutrient utilization characteristics of low-light adapted *Prochlorococcus*, high-light adapted *Prochlorococcus*, *Synechococcus*, autotrophic eukaryotes, and large diatoms. The simulated response of the lower trophic levels in the two regions of the equatorial Pacific to ENSO cycles differs in community structure and level of production. For the Cold Tongue region, the ENSO warm phase results in a shift to small algal forms (e.g., *Prochlorococcus* spp. and *Synechecoccus*) and low primary productivity (25 mmol C m^{-2} d^{-1} versus an annual average of 75 mmol C m^{-2} d^{-1}). For the Warm Pool region, the phytoplankton community is dominated by larger algal forms (e.g., autotrophic eukaryotes) and primary production increases (150 mmol C m^{-2} d^{-1} versus an annual average of 59 mmol C m^{-2} d^{-1}). Also, during ENSO events carbon production and export in the Cold Tongue are limited by iron, whereas the relative abundance of iron and macronutrients (i.e. nitrate, silicate) limits production and export in the Warm Pool. Model results suggest that the occurrence of the large bloom following the 1997 El Niño at 140°W cannot be explained by local processes and that resolving the so called "barrier layer" is critical to simulate the biological dynamics at 165°E. Inclusion of diurnally varying mixed layer depths did not greatly affect the simulated carbon export. This suggests that pumping of particulate material out of the euphotic zone due to mixed layer shoaling during the day and redistribution of particulate material throughout the mixed layer due to mixed layer deepening during the night can be counter balanced.

1. Introduction

During the 1990s the equatorial Pacific was characterized by active El Niño-Southern Oscillation (ENSO) variability that included 3 El Niño episodes (1991–1993, 1994–1995, and 1997–1998) and 2 La Niña episodes (1995–1996, 1998–1999). This period also featured the strongest El Niño episode of the century (1997–1998) (McPhaden, 1999), as well as two consecutive periods of El Niño conditions during 1991–1995 without an intervening cold episode.

Observations of biogeochemical variability associated with ENSO variability are limited. The massive event of 1997–1998

---

* Center for Coastal Physical Oceanography, ODU, Norfolk, VA, United States.
E-mail address: baris@ims.metu.edu.tr.

0924-7963/$ – see front matter © 2008 Elsevier B.V. All rights reserved.
doi:10.1016/j.jmarsys.2008.12.004

Please cite this article as: Salihoglu, B., Modeling the effect of ENSO on the lower trophic level ecosystem of the Cold Tongue and the Warm Pool regions in the equatorial Pacific, Journal of Marine Systems (2009), doi:10.1016/j.jmarsys.2008.12.004

is the only one observed synoptically by ocean color sensors (Murtugudde et al., 1999). U.S., French, Australian and Japanese investigations in the western and central equatorial Pacific occurred throughout the 1990s which provide observations of the equatorial ocean in a variety of ENSO states (Murray et al., 1995; Radenac and Rodier, 1996; Ishizaka et al., 1997; Mackey et al., 1997; Dunne et al., 2000; Strutton and Chavez, 2000; Aufdenkampe et al., 2001; Aufdenkampe and Murray, 2002; Le Borgne et al., 2002).

The equatorial Pacific, which is the primary locus of ENSO, is subject to physical forcings that differ markedly from east to west. The Cold Tongue in the east (centered near 0°N, 140°W Murray et al., 1992) is subject to the divergence of the South Equatorial Current (SEC). Such a divergence generates upwelling of the waters from the Equatorial Undercurrent (EUC), which bring waters with higher salinity, dissolved inorganic carbon and nutrient concentrations to the surface.

In spite of upwelling which provides nutrients to the upper water column, this portion of the equatorial Pacific is characterized by modest chlorophyll concentrations and low rates of primary production (PP) of about 0.2 to 0.3 $\mu g\ l^{-1}$ and 75 mmol C $m^{-2}\ d^{-1}$, respectively (Chavez et al., 1999). This high-nutrient, low-chlorophyll (HNLC) environment has been attributed to low iron concentration (Martin et al., 1994; Coale et al., 1996a,b; Barber et al., 1996) and high zooplankton grazing rates (Walsh, 1976; Cullen et al., 1992; Landry et al., 1997).

In contrast, the Warm Pool region in the western equatorial Pacific (centered near 0°N, 165°E) is characterized by some of the warmest sea surface temperatures (SSTs) (annual mean of 28 °C to 30 °C) in the global ocean and has a shallow mixed layer (30–40 m) separated from the thermocline (deeper than 65 m) by a high-salinity barrier layer (Lukas and Lindstrom, 1991). Mackey et al. (1995) and Radenac and Rodier (1996) emphasize that the suppression of nutrient fluxes by the salinity barrier layer controls surface phytoplankton concentrations in the Warm Pool. Despite differences in physical and chemical forcings between the Warm Pool and the Cold Tongue, the depth-integrated chlorophyll concentrations in the Cold Tongue (25–36 mg m^{-2}) region are only slightly higher than those observed in the Warm Pool under normal or El Niño conditions (20–30 mg m^{-2}, Mackey et al., 1997). However, the availability of biological observations for the Warm Pool region is considerably less than for the Cold Tongue region.

The manifestation of the ENSO is also different in two regions. Under non El Niño conditions, the trade winds pile up water in the western equatorial Pacific, resulting in an increase in sea level and deepening of the thermocline (Wyrtki, 1975, 1985). When the trade winds weaken, these perturbations of the thermocline and the sea surface can propagate eastward as downwelling Kelvin waves. These waves carry energy across the basin rapidly, resulting in a depression of the thermocline and a warming of the sea surface in the east, which in turn results in weakening of the trade winds (Philander, 1990; Hansen, 1990). The equatorial Pacific then takes on a self-sustaining state characterized by warm surface temperatures, weak trade winds, a weak or reversed SEC, and a significantly reduced east–west slope of the sea surface, which results in the attenuation and occasional disappearance of the EUC (Firing et al., 1983). The depth of the thermocline, the main reservoir of nutrients for phytoplankton, is deeper than usual in the east and shallower in the west. In the western equatorial Pacific the shoaling of the thermocline during El Niño which brings the nutrients into the euphotic zone, causes an increase in the chlorophyll concentration in the deep chlorophyll maxima layer (Blanchot et al., 1992; Radenac and Rodier, 1996).

The main focus of this study is to investigate the response of the equatorial Pacific biogeochemistry to dynamical forcing associated with ENSO. This investigation is done using an algal group based complex ecosystem model that was developed for the Cold Tongue (Salihoglu and Hofmann, 2007). This model was adapted for the Warm Pool region, which allows comparisons between the region and the Cold Tongue that are based on a similar model structure.

The model is used to address questions regarding the effect of ENSO on PP, biomass and export production in the Cold Tongue and the Warm Pool regions. Specifically, the model is used to focus on limiting nutrients and uncertainties regarding the abundance and distribution of dissolved iron. Sensitivity tests are carried out to test the influence of time-variable iron deposition and diurnally-varying mixed layer depths on the ecosystem of the Cold Tongue.

The next section gives a summary of the lower trophic level model used in this study and the data sets input to the model. The results of the simulations for the Cold Tongue and the Warm Pool are given in Section 4. Section 5 discusses the results within the current understanding of the factors controlling lower trophic level production in the eastern and western equatorial Pacific. The final section gives the conclusions derived from this study.

2. Data sources and procedures

2.1. Vertical velocity, diffusion, and mixing

The one-dimensional lower trophic level ecosystem model, described in Section 3, includes explicit effects of vertical advection. The approach taken here is to use direct observations of the horizontal velocities (u and v) and temperature obtained from the Tropical Ocean-Global Atmosphere (TOGA) program and the Tropical Atmosphere-Ocean (TAO) Array, which were obtained from moorings/buoys at fixed locations in the equatorial Pacific Ocean. Details of the TAO Array are given in McPhaden et al. (1998) and data from the mooring are available via the TAO web-site (http://www.pmel.noaa.gov/toga-tao).

The TAO mooring array provides time series of current meter-measured horizontal velocity and temperature at locations along the equator at 156°E, 165°E, 180°W, 155°W, 140°W, and 125°W, and along 140°W and 165°E at 2°N, and 2°S. The vertical distribution of the velocity and temperature measurements is sufficient to resolve variations in the upper water column environmental structure caused by high-frequency events, such as Tropical Instability Waves (TIWs) and Internal Gravity Waves (IGWs), and low frequency events such as ENSO.

Throughout 1991–1999, the data availability is 90% or more for horizontal velocity and temperature at 0°N, 140°W, respectively and is 90% or more for horizontal velocity and 80% or more for temperature at 0°N, 165°E. The periods of

Please cite this article as: Salihoglu, B., Modeling the effect of ENSO on the lower trophic level ecosystem of the Cold Tongue and the Warm Pool regions in the equatorial Pacific, Journal of Marine Systems (2009), doi:10.1016/j.jmarsys.2008.12.004

missing data are filled in by averaging the equivalent measurements from TAO moorings at 2°N and 2°S at 140°W and 165°E. For times when no measurements are available from any of the sites, the data are linearly interpolated in time using the available points on either side of the data gaps. The resultant daily time series is then linearly interpolated to 1-hour intervals to be consistent with the time step used for the lower trophic level ecosystem model (cf. Section 3.1).

The temperature and horizontal velocity time series from the TAO Array for 1991–1999 are used with the procedure given in Friedrichs and Hofmann (2001) to estimate vertical velocities. This approach is based on scaling vertical velocity relative to local upward movement of an isotherm and advection along a stationary, sloping isotherm. Daily estimates of local upward movement of the isotherms are obtained by evaluating the change in the depths of the isotherms measured by the TAO temperature sensors. The advection along a stationary, sloping isotherm is computed by multiplying zonal velocity data, measured by the TAO current meters, by estimates of zonal isotherm slopes.

The mixed layer depth is set to the depth where water temperature is 1°C lower than the SST. The comparisons between the mixed layer depths observed during the U.S. JGOFS cruises and the mixed layer depths estimated using 1 °C difference from the observed SSTs give very satisfactory results at 0°N, 140°W (Salihoglu, 2005).

The mixed layer depth at 0°N, 140°W is estimated using the hourly temperature measurements to incorporate the diurnal variability in the mixed layer depth, whereas daily temperature values are used at 0°N, 165°E. The vertical diffusion (K_z) effects are simulated with a theoretical model (Pacanowski and Philander, 1981) using the TAO mooring (u, v, T) observations. All of the components (e.g., state variables) of the lower trophic level model are homogeneously distributed in the mixed layer at each time step.

2.2. Shortwave radiation

The TAO mooring at 0°N, 140°W and 0°N, 165°E provides time series of integrated incoming short wave radiation. For 1991–1999, this record is about 85% complete at 0°N, 140°W and is about 75% complete at 0°N, 165°E. The missing portions of the shortwave radiation time series are estimated from either adjacent moorings or linear interpolation between available data points, similar to what is done for the horizontal velocities. When there are no data available from all the three sites, the effect of cloud cover is neglected. The resultant shortwave radiation time series is used with a clear sky radiation model to estimate the spectrally-resolved underwater light field (cf. Salihoglu and Hofmann, 2007).

2.3. Warm Pool in situ observations

Observations that can be used to describe the distributions and rates of the lower trophic levels in the Warm Pool are considerably limited relative to those available for the Cold Tongue. The observations from U.S. JGOFS Equatorial Pacific process study (Murray et al., 1994, 1995) are used for model evaluation in the Cold Tongue region for year 1992 (Salihoglu and Hofmann, 2007) and will not be repeated here. As part of the JGOFS study of the equatorial Pacific, two stations are occupied at 0°N, 165°E as part of the FLUPAC and Zonal Flux cruises (Rodier and Le Borgne, 1997; Aufdenkampe and Murray, 2002; Dunne et al., 2000; Le Borgne et al., 2002), which occurred in September–October 1994 and April 1996, respectively. Observations made during the FLUPAC and Zonal Flux cruises provide measurements of macronutrients (nitrate, ammonium, silicate), chlorophyll *a* concentration and primary production.

Data collected during the FLUPAC and Zonal Flux cruises are used for the model-data comparisons in the Warm Pool region at 0°N, 165°E (Section 4). The samples that were collected at the nominal depths are linearly interpolated to 1-m depth intervals to for comparison with the corresponding simulated distributions.

2.4. Satellite-derived ocean color measurements

The Sea-viewing Wide Field of view Sensor (SeaWiFS) data used in this analysis are daily composites, averaged over a 2° longitude by 2° latitude rectangle centered on 0°N, 140°W and 0°N, 165°E. The time-series begins with the first reliable retrieval on September 1997 and continues through February 1999. Strong ENSO conditions are present throughout the 1997–1998 portion of the data. The SeaWiFS surface chlorophyll *a* data are used for the model-data comparison in the Cold Tongue (Sections 4.1.2 and 5.2) and the Warm Pool (Sections 4.3.2 and 5.2) regions.

3. Model structure

Details of the lower trophic level model are given in (Salihoglu and Hofmann, 2007) and are described only briefly here. In this study a one-dimensional, algal group-based phytoplankton model is used to simulate phytoplankton dynamics in the upper 120 m of equatorial Pacific Ocean (Fig. 1). The phytoplankton model is part of a lower trophic level ecosystem model that is coupled to a larger model structure that provides the external forcing fields for all state variables as described below.

The simulated surface light field, which provides input to the underwater light field is obtained from a clear sky spectral irradiance model (Gregg and Carder, 1990) that is corrected for cloud cover effects using the shortwave radiation measurements from the TOGA TAO observations. The spectral attenuation of light energy with increased water depth is estimated as a function of the spectral absorption and backscattering of the water and particulate materials and used to force the full-spectral, algal group-based phytoplankton model. The pigment concentrations estimated for each algal group in the phytoplankton model are used to estimate particulate material concentration as a feedback into the bio-optical model.

The effects of the physical environment are included in the ecosystem model using the advective velocity and temperature time series from the TAO mooring. Similarly the time varying mixed layer depth obtained from the TAO mooring measurements and the theoretically derived vertical diffusion coefficients are input into the ecosystem model. The comparisons between the mixed layer depths observed during the U.S. Joint Global Ocean Flux Study (JGOFS) cruises and the mixed layer depths estimated using 1°C difference from the

Please cite this article as: Salihoglu, B., Modeling the effect of ENSO on the lower trophic level ecosystem of the Cold Tongue and the Warm Pool regions in the equatorial Pacific, Journal of Marine Systems (2009), doi:10.1016/j.jmarsys.2008.12.004

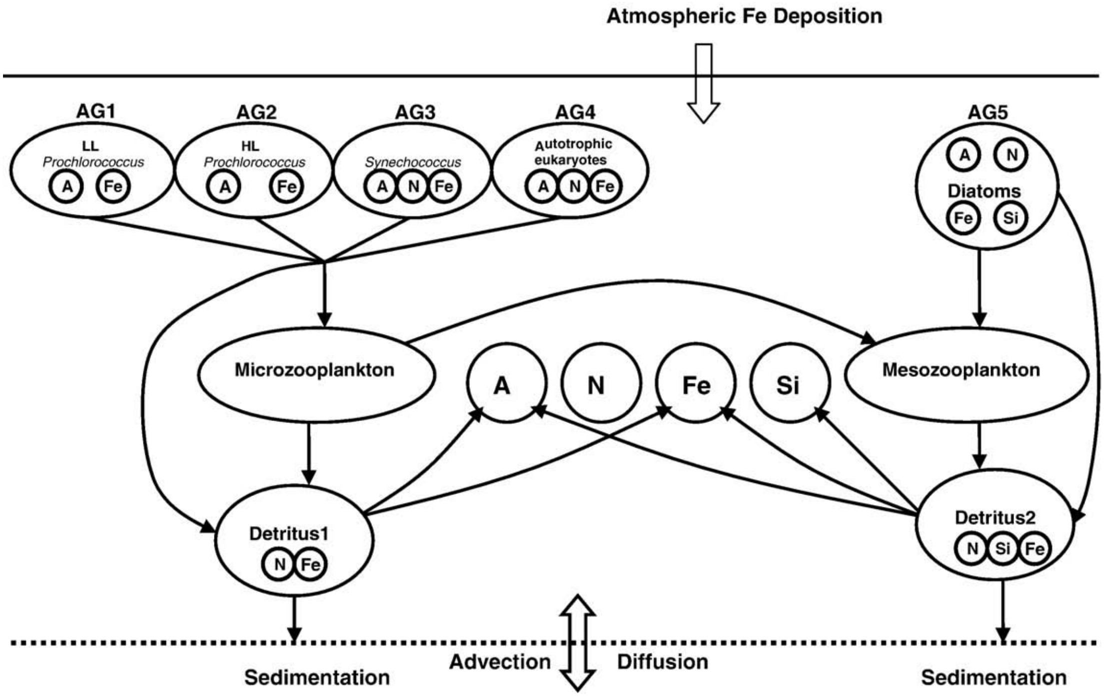

Fig. 1. Schematic of the lower trophic level ecosystem model components. Small circles inside the big circles indicate the internal nutrient compartments of each algal and detrital group. Interactions between nutrient, phytoplankton, zooplankton, and detritus compartments are shown by solid lines and arrows. Small arrows indicate the direction of transfer between model compartments; whereas, open arrows indicate the direction of transfer at the boundaries. Upper model boundary is indicated by a solid line, and it is only open to aeolian iron deposition. The bottom boundary is an open boundary which is indicated by a dotted line. Abbreviations used are: AG — algal group; LL — low light-adapted; HL — high light-adapted; A — ammonium; N — nitrate; Fe — iron; Si — silicate.

observed SSTs gives very satisfactory results at 0°N, 140°W (Salihoglu, 2005).

Atmospheric (aeolian) deposition of iron provides another input for the lower trophic level ecosystem model because iron is believed to limit phytoplankton growth in equatorial Pacific waters. Aeolian iron deposition is estimated using the monthly atmospheric dust flux, which is obtained from Ginoux et al., (2001).

The phytoplankton algal groups (*AG*) included as state variables in the ecosystem model represent the dominant autotrophic biomass in the equatorial Pacific as determined from pigment and size fractional studies (Chavez, 1989; Iriarte and Fryxell, 1995; Lindley et al., 1995; Bidigare and Ondrusek, 1996; Chavez et al., 1996; Coale et al., 1996b; Landry et al., 1996, 2000; Latasa et al., 1997; Higgins and Mackey, 2000) and are sufficient to represent over 90% of the equatorial Pacific phytoplankton biomass. The accessory pigments included in the model are categorized as chlorophyll *a*, chlorophyll *b*, chlorophyll *c*, photosynthetic carotenoids, photoprotective carotenoids, and phycoerythrin. The five algal groups represent low-light adapted *Prochlorococcus* (*AG*1), high-light adapted *Prochlorococcus* (*AG*2), *Synechococcus* (*AG*3), autotrophic eukaryotes (*AG*4) and microplankton (large diatoms, *AG*5).

Recent observations show that both nitrogen and iron can potentially limit primary production in the eastern and central equatorial Pacific Ocean (Martin et al., 1990, 1991; Price et al., 1994; Behrenfeld et al., 1996; Coale et al., 1996a; Landry et al., 1997, 2000) and that silicate limits diatom growth (Dugdale and Wilkerson, 1998). This understanding is included in the formulations used for growth of the five algal groups, which incorporates uptake of ammonium, nitrate, iron, and silicate. All of the algal groups use ammonium and iron; whereas, nitrate is only used by algal groups 3, 4, and 5. Silicate is only used by algal group 5.

The specific rates of phytoplankton nutrient uptake and growth can be uncoupled depending upon the nutritional status of the phytoplankton cell (Droop, 1973; Goldman, 1980, 1982; Goldman and Glibert, 1983). This study has objectives that focus on understanding the effects of physical and biological processes on phytoplankton community composition and nutrient dynamics in the equatorial Pacific. Therefore, the nutrient limited growth rate of algal groups is formulated using separate parameterizations for nutrient uptake and growth rates (cf. Salihoglu and Hofmann, 2007 for details). Each algal group has cellular carbon, nitrogen (ammonium + nitrate), and iron compartments and algal group 5 has a cellular silicate compartment. The phytoplankton cellular nitrogen, iron, and silicate are needed to calculate uptake of nitrogen, iron and silicate by phytoplankton and to estimate nitrogen-, iron- and silicate-limited growth rates.

Two groups of zooplankton are included in the ecosystem model which represent microzooplankton and mesozooplankton. Microzooplankton graze on *Prochlorococcus* spp., *Synechococcus*, and autotrophic eukaryotes. The mesozooplankton graze on large diatoms and microzooplankton (Dam et al., 1995; Landry et al., 1995; Zhang et al., 1995; Verity et al., 1996).

The detrital component of the ecosystem model is divided into small and large detritus groups. Detrital components are

Please cite this article as: Salihoglu, B., Modeling the effect of ENSO on the lower trophic level ecosystem of the Cold Tongue and the Warm Pool regions in the equatorial Pacific, Journal of Marine Systems (2009), doi:10.1016/j.jmarsys.2008.12.004

split into two groups because each group has unique sinking and remineralization rates (Nelson et al., 1995; Laws et al., 2000). The small detrital pool receives input from algal groups 1–4 that result from losses due to non-grazing mortality. Additional inputs to this detrital pool are from microzooplankton excretion and fecal pellet production (unassimilated ingestion). Losses by algal group 5 from non-grazing mortality and mesozooplankton excretion and fecal pellet production provide the inputs to the large detrital pool. Remineralization of small and large detritus provide sources of ammonium and iron (Laws et al., 2000). Dissolution of silicate in the large detritus compartment provides a source for this nutrient (Nelson et al., 1995). The detritus compartments are allowed to sink at a fixed rate.

The ambient nutrient concentrations are an integral component of the dynamics governing the nutrient uptake by each algal group as described above. The nitrogen is partitioned into two components, recycled nitrogen, ammonium, and new nitrogen, nitrate. In the model it is assumed that the only biological process that regulates nitrate concentration is uptake by algal groups. However, the ammonium concentration is modified through the uptake by each algal group, excretion by microzooplankton, excretion by mesozooplankton, and remineralization of small detrital nitrogen and large detrital nitrogen. The remineralization rate of detrital nitrogen to ammonium, is assumed to be modified by temperature (cf. Salihoglu and Hofmann, 2007 for details). The iron dynamics are assumed to be governed similar to ammonium except for a surface deposition term and a scavenged iron term. The remineralization rate of detritus to iron is also assumed to vary as a function of temperature. The particle scavenging iron loss term is adopted from Moore et al. (2002). The processes that affect silicate concentration are similar to nitrate except for the addition of silicate through dissolution of large detritus silicate.

3.1. Model implementation

3.1.1. Numerical methods

The one-dimensional lower trophic level model is implemented with a coordinate system with the origin at the sea surface and the vertical coordinate positive downward. The model domain extends from the sea surface to 120 m, which is below the 1% light level. This is sufficiently deep to include the total phytoplankton production in the upper waters of the equatorial Pacific.

The vertical coordinate is represented at 1-m intervals, which is sufficient resolution to define features such as the deep chlorophyll maximum that occurs in equatorial Pacific waters (Lindley et al., 1995). A one-hour interval is used for the time integration, which allows resolution of the diurnal periodicity in phytoplankton growth kinetics. The model is initially run for 1 year using bottom initial conditions as the repeating forcing to bring the model to steady-state.

3.1.2. Surface and bottom boundary conditions

Surface boundary conditions were specified as no flux conditions (i.e. Neumann conditions) for all model state variables except for iron. For iron, the daily atmospheric dust flux in g m^{-2}, obtained from Ginoux et al. (2001), is used to specify an input at 0°N, 140°W and 0°N, 165°E. This input is specified from the sum of four dust size classes (0.1–1, 1–2, 2–3 and 3–6 μm). The mass fraction of iron in the mineral dust aerosol is assumed to be 0.05 for the first size class and 0.012 for the remaining size classes (Fung et al., 2000). The soluble iron fraction is taken to be 0.1 (Duce et al., 1991; Duce and Tindale, 1991). The dust flux in g m^{-2} day^{-1} is converted to a flux in nmol l^{-1} hr^{-1} by using appropriate scaling factors. It is assumed that the dust deposited on 1 m^2 at the sea surface is introduced to a 1 m^3 water volume. At each time step this surface concentration is homogeneously distributed in the mixed layer.

3.1.2.1. Cold Tongue.

The bottom boundary conditions for nitrate, silicate and iron are specified using a temperature-nutrient relationship in the Cold Tongue. The nitrate (NO_3^-) and iron (Fe) dependencies on temperature (*T*) are taken from Barber and Chavez (1991) and Leonard et al. (1999), respectively, and are given as

$$NO_3^-(z,t) = 66.70 - 3.90T(z,t) + 0.06T(z,t)^2, \tag{1}$$

$$\mathrm{Fe}(z,t) = 0.50 - 0.019T(z,t), \tag{2}$$

where NO_3^- and Fe are in μmol l^{-1} and nmol l^{-1}, respectively. The depth and time varying temperature is obtained from the time series measured at TAO mooring arrays.

A silicate (Si) to temperature (*T*) regression is developed using data from four 1992 U.S. JGOFS EqPac cruises:

$$\mathrm{Si}(z,t) = 26.35 - 0.90T(z,t). \tag{3}$$

An ammonium-to-temperature relationship does not exist and therefore the Christian et al. (2002a) simulation is used to set the ammonium bottom boundary conditions at 120 m.

3.1.2.2. Warm Pool.

The nitrate-to-temperature and silicate-to-temperature regressions at 120 m are estimated using the climatological data at 0°N, 165°E from Conkright et al. (2002) as

$$NO_3^-(z,t) = 35.39 - 1.18T(z,t) \tag{4}$$

and

$$\mathrm{Si}(z,t) = 15.9 - 0.50T(z,t), \tag{5}$$

where NO_3^- and Si are in μmol l^{-1}.

The iron to temperature regression is similar to the iron-to-temperature regression developed for 0°N, 140°W. For 0°N, 165°E, the regression coefficients are modified to match the corresponding temperatures at 120 m as

$$\mathrm{Fe}(z,t) = 0.499 - 0.013T(z,t), \tag{6}$$

where Fe is in nmol l^{-1}.

The Christian et al. (2002a) simulation are used to set the ammonium bottom boundary conditions at 120 m.

3.1.3. Initial vertical profiles

Initial profiles of phytoplankton, small and large zooplankton and detritus, and ammonium are obtained from the

Please cite this article as: Salihoglu, B., Modeling the effect of ENSO on the lower trophic level ecosystem of the Cold Tongue and the Warm Pool regions in the equatorial Pacific, Journal of Marine Systems (2009), doi:10.1016/j.jmarsys.2008.12.004

Christian et al. (2002a) simulation at 20 depth intervals and linearly interpolated to 1-m depth intervals. The small and large phytoplankton compartments obtained from the Christian et al. (2002a) simulation are partitioned into 5 algal groups based on the relative ratios of these algal groups measured during the U.S. JGOFS cruises (Landry et al., 1996; Iriarte and Fryxell, 1995). The initial profiles of nitrate, iron, and silicate are estimated using the nutrient to temperature relations. Very small (0.0001 μmol C l^{-1}) threshold values are set for the phytoplankton and zooplankton state variables, so that these concentrations do not become zero. This provides a refuge for these ecosystem components so they can respond when conditions become favorable for growth.

4. Results

4.1. Cold Tongue simulations (1991–1999)

The ecosystem model described in Section 3 is implemented at 0°N, 140°W (the Cold Tongue region) to do a simulation for 1991–1999 (~8-years), which involves three El Niño events and two La Niña events. The TAO data that are used to construct the environmental time series that are input to the model are almost continuous during this time. Equivalent 8-year simulations are done for the Warm Pool (0°N, 165°E) for comparison (cf. Section 4.3). The Southern Oscillation Index (SOI), which is a measure of large-scale fluctuations in air pressure between the western and eastern tropical Pacific (Trenberth and Hoar, 1996), is used to determine the warm and cold ENSO phases for 1991–1999. Because the ecosystem model is evaluated for the Cold Tongue region (Salihoglu and Hofmann, 2007) using the 1992 U.S. JGOFS Equatorial Pacific process study (EqPac) data (Murray et al., 1994, 1995) only model-data comparisons done with SeaWiFS derived chlorophyll *a* data are given here (cf. Section 4.1.2).

4.1.1. Cold Tongue environmental time series

The temperature time series (Fig. 2A) obtained at 0°N, 140°W from the TAO mooring shows prolonged periods of negative SOI values that coincide with abnormally warm (>28 °C, at the surface) ocean waters, which are typical of El Niño conditions (Philander, 1990). Conversely, prolonged periods of positive SOI values coincide with abnormally cold (<24 °C, at the surface) ocean waters, indicating typical La Niña conditions.

The temperature and SOI time series (Fig. 2A) show that the strongest recorded ENSO starts after February 1997. The SOI stays negative until the beginning of 1998, and the surface waters remain near 30 °C for almost a year. During this period the surface ocean is completely stratified with warm (30 °C) waters extending to 120 m. Towards the end of 1997 the system starts to shift into a La Niña phase, and the coldest surface temperatures (~20 °C) of the decade are observed during 1998.

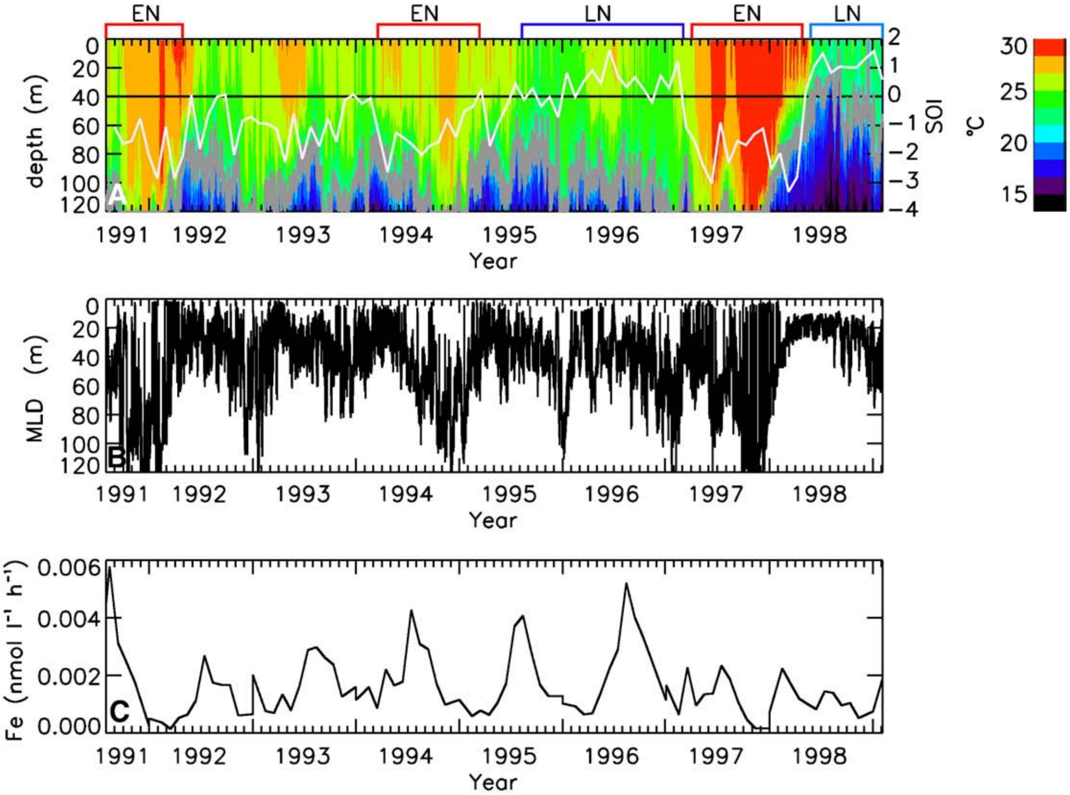

Fig. 2. (A) Depth-time distribution of temperature, time series of (B) estimated mixed layer depth (MLD) and, (C) aeolian iron flux (Ginoux et al., 2001) for 1991 to 1999. The temperature and mixed layer depth are from the TAO mooring at 0°N, 140°W. The Southern Oscillation Index (SOI), obtained from the U.S. Department of Commerce National Oceanic and Atmospheric Administration (http://www.elnino.noaa.gov/) is shown in panel A (white line) relative to the zero SOI (black line). The 20 °C isotherm is shown in panel A (light grey line). The time periods of El Niños (EN, red) and La Niñas (LN, blue) are shown.

Please cite this article as: Salihoglu, B., Modeling the effect of ENSO on the lower trophic level ecosystem of the Cold Tongue and the Warm Pool regions in the equatorial Pacific, Journal of Marine Systems (2009), doi:10.1016/j.jmarsys.2008.12.004

The buildup and waning of 1991–1992 and 1997–1998 El Niños show similar characteristics. At the beginning of the 1991–1992 and 1997–1998 El Niños the warming of the surface waters occurred rapidly and warm waters immediately penetrated to 100 m deep. However, cooling is more gradual, and the subsurface waters, around 120 m, start to cool in the middle of the El Niño event and cold waters reach ~60 m before the buildup of the cold episodes.

The time series of temperature (Fig. 2A) can also give indications about the state of the EUC (light grey line). The EUC is generally indicated by temperatures between 15°C and 20°C in the equatorial Pacific (Halpern, 1980; Tomczak and Godfrey, 1994). The temperature time series show that the EUC (Fig. 2A, light grey line) is missing within the euphotic zone during the three El Niño events (1991, 1994, and 1997). However, during the cold phases of the ENSO, the temperatures at 120 m are below 20°C indicating the intrusion of the EUC into the euphotic zone. In particular during the 1997 La Niña the 20°C isotherm intersected the sea surface, indicating that during this period, EUC is reaching the sea surface (Yu and McPhaden, 1999).

The mixed layer depths (Fig. 2B), are persistently shallow throughout 1998, which corresponds to the strong La Niña episode. A sharp decrease in mixed layer depth occurs towards the end of 1997, and during 1998 the mixed layer depth stays at ~20 m, and shows little variation. The shoaling of mixed layer depths during the cold phases is the result of shoaling of the isotherms during these periods.

The aeolian iron flux obtained from Ginoux et al. (2001) indicates a strong annual variability in iron deposition (Fig. 2C). The lowest deposition occurs during February–April and the highest during August–October. Years 1991 and 1996 correspond to a high dust deposition period and in 1992 and 1998 iron deposition is low.

The simulated downwelling irradiance field shows that the SOI strongly influences the cloud cover in Cold Tongue region (not shown, cf. Salihoglu, 2005). During times of strong negative SOI, cloud cover can reduce the intensity of the surface irradiance by 80%. The strongest effect of cloud cover on the downwelling irradiance is observed during the 1992 and 1997–1998 El Niño events. While the cloud cover can significantly reduce the irradiance, its effect on the depth of the euphotic zone is minimal, producing only a 3 m decrease in the euphotic zone depth during high cloud cover periods.

4.1.2. Phytoplankton

The simulated primary production at 0°N, 140°W for 1991 to 1999 (Fig. 3) shows that the transition periods between El Niño and La Niña events are the times of greatest change in primary production. The times of negative change in the SOI coincide with low simulated primary production values (Fig. 3). The lowest primary production values occur during the 1997 (10 mmol C m^{-2} d^{-1}), 1992 (12 mmol C m^{-2} d^{-1}), and 1995 (20 mmol C m^{-2} d^{-1}) El Niño events. Once the SOI starts to shift towards positive, the simulated primary production begins to increase and reaches values that are about a factor of 6 greater than those during the negative SOI phase.

The recovery from El Niño conditions begins prior to full development of La Niña conditions. Observations show that the intrusion of cold waters into the euphotic zone starts ~4 months before the SOI turns positive (Fig. 2A). During this period the estimated mixed layer depth is still deep compared to the post El Niño phases (Fig. 2B). This combination of cold water intrusion with deep mixed layers introduces nutrients, especially iron in the surface waters, and results in the simulated La Niña bloom at the time when the SOI shifts towards positive (Fig. 3). During periods of persistently high SOI, such as during 1996 and early 1997, the algal groups can sustain high primary production rates.

The physiological differences among algal groups, which are included in the model structure (Section 3), determine the differences in their spatial and temporal distribution. The simulated distributions of the five algae groups at 0°N, 140°W for 1991–1999 (Fig. 4A–E) show that algal groups 2 to 4 bloom during the end of the negative phases of SOI. The times of highest biomass of algal groups 1 and 5 coincide with low biomass periods of other groups. Algal group 4 dominates the algal biomass at all times (Fig. 4).

In the 8-year simulation, maxima in algal group 1 biomass occur below the mixed layer (Fig. 4A) and maxima of algal group 2 occur in the mixed layer (Fig. 4B). *Synechococcus* spp. (algal group 3) is less abundant compared to *Prochlorococcus* (algal groups 1+2, Fig. 4C), with the average water column biomass of the two being 21 mmol C m^{-3} and 41 mmol C m^{-3},

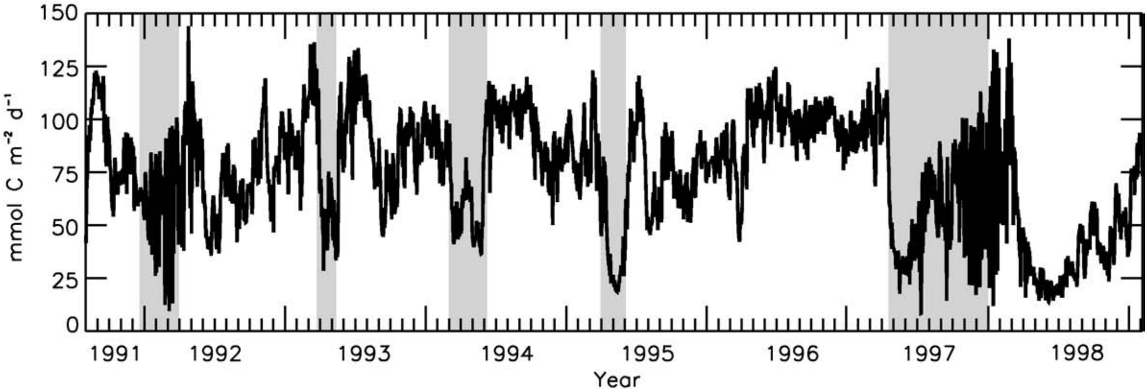

Fig. 3. Simulated time distribution of primary production integrated over the water column (120 m) in the Cold Tongue. Shaded regions denote the peak periods of the negative phases of the SOI.

Please cite this article as: Salihoglu, B., Modeling the effect of ENSO on the lower trophic level ecosystem of the Cold Tongue and the Warm Pool regions in the equatorial Pacific, Journal of Marine Systems (2009), doi:10.1016/j.jmarsys.2008.12.004

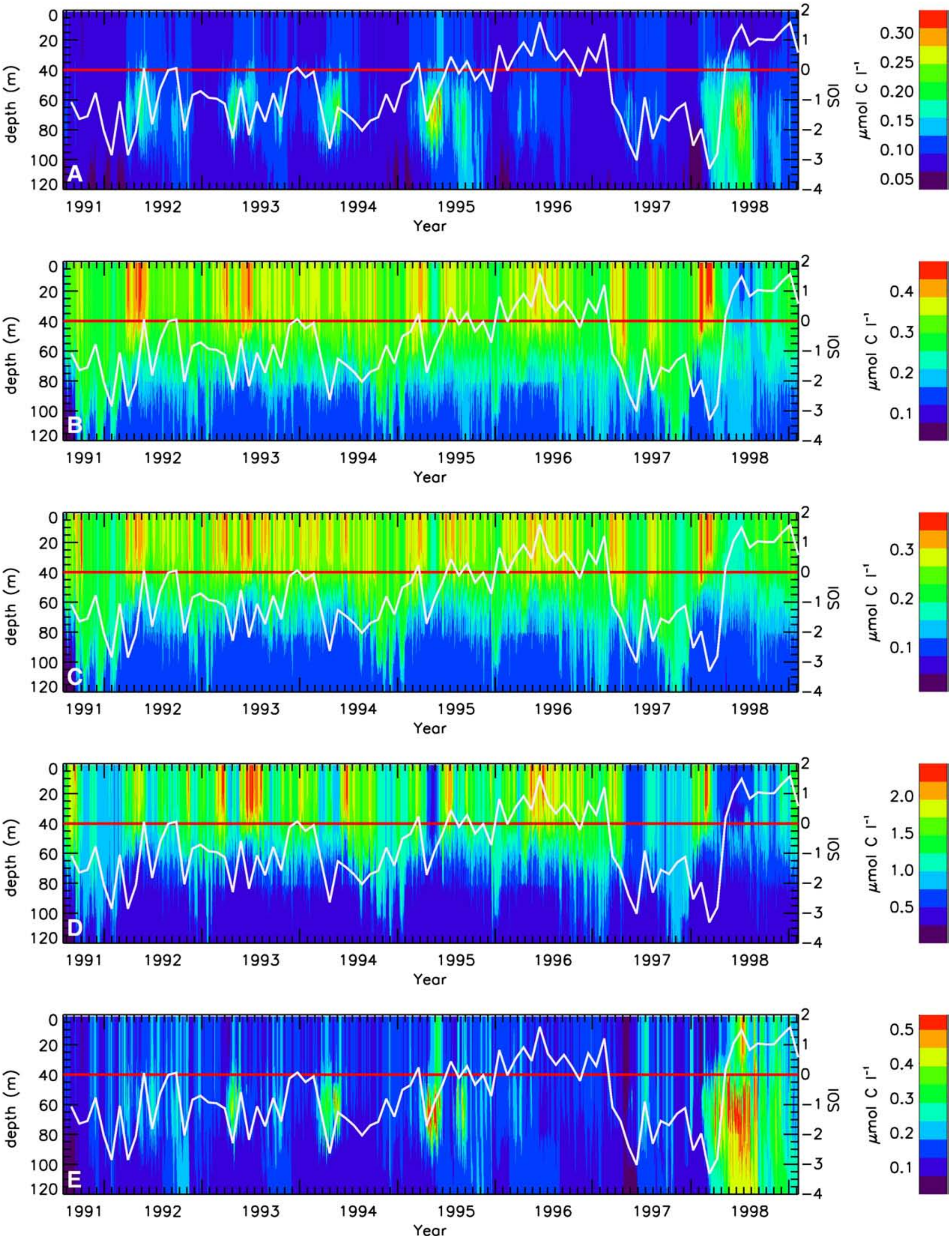

Fig. 4. Simulated depth–time biomass (μmol C l^{-1}) distributions of (A) low light-adapted *Prochlorococcus* (algal group 1), (B) high light-adapted *Prochlorococcus* (algal group 2), (C) *Synechococcus* (algal group 3), (D) autotrophic eukaryotes (algal group 4), and (E) large diatoms (algal group 5) in the Cold Tongue region at 0°N, 140°W. The color scales for each group are different. The SOI is shown (white line) relative to the zero SOI (dashed line).

Please cite this article as: Salihoglu, B., Modeling the effect of ENSO on the lower trophic level ecosystem of the Cold Tongue and the Warm Pool regions in the equatorial Pacific, Journal of Marine Systems (2009), doi:10.1016/j.jmarsys.2008.12.004

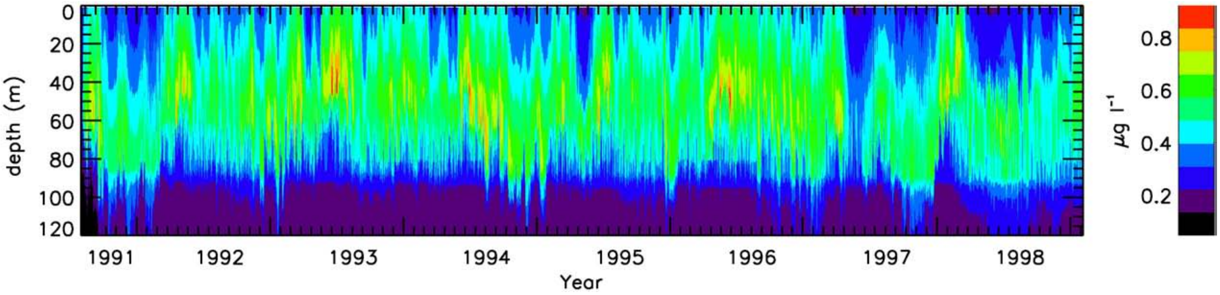

Fig. 5. Simulated depth-time distribution of chlorophyll *a* (μg l^{-1}) at 0°N, 140°W obtained from the sum of all five algal groups.

respectively. The majority of the biomass of algal group 4 is at depths shallower than 45 m (Fig. 4D) and that for algal group 5 is at depths deeper than 45 m (Fig. 4E).

The simulated time-depth distribution of chlorophyll *a* concentrations obtained from the sum of all five algal groups (Fig. 5) shows that chlorophyll *a* in the mixed layer varies from 0.3 to up to 1.0 µg l^{-1} on interannual time scales. A deep chlorophyll maximum is always present at 0°N, 140°W even during the 1997 El Niño period, when surface chlorophyll *a* values are particularly low (<0.2 µg l^{-1}). During the eight-year simulation there are 10 periods where the surface chlorophyll *a* values are above 0.6 µg l^{-1} (e.g., May–July 1993, March 1998) (Fig. 5). The deep chlorophyll maximum concentrations at these times are ~0.8 µg l^{-1} (Fig. 5). Also, there are periods with subsurface chlorophyll *a* values of ~0.8 µg l^{-1}, which correspond to surface chlorophyll *a* values below 0.4 µg l^{-1} (e.g., April 1998, Fig. 5). The comparison of simulated mixed layer averaged chlorophyll *a* versus SeaWiFS chlorophyll *a* (Fig. 6) shows that although average chlorophyll *a* values compare well (black dots) the simulated values during the El Niño period overestimate the observed values. This misfit is at odds with the good model-data comparison obtained for the 1992 ENSO (Salihoglu and Hofmann, 2007). The possible reasons for this misfit are discussed in detail in Section 5.2.

Because chlorophyll *a* represents the balance between production and grazing (Landry et al., 1997) the effect of grazing is also analyzed. Simulation results show that tight coupling between primary production and grazing exists during both high productivity and lower productivity periods. For example, during the first 3 months of 1997 (Fig. 5) the total daily primary production is 99 mmol C m^{-2} d^{-1} whereas during 1997 El Niño it is almost half this value (55 mmol C m^{-2} d^{-1}). However, during both periods the part of algal production that is removed by grazing is around 90%.

4.1.3. Nutrients

The simulated distributions of the three macronutrients and one micronutrient in the upper 120 m at 0°N, 140°W are low during the El Niño periods and high during the La Niña periods (Fig. 7A–D). The lowest nutrient concentrations occur during the middle of the warm El Niño periods (negative SOI) after which they increase towards the end of the negative phase of SOI. All nutrients are close to depletion during the 1997 El Niño and concentrations are especially low during the 1991 and 1994 El Niño periods (Fig. 7A–D). Nitrate, iron, and silicate reach their highest values during the initial part of the positive SOI phases. The highest simulated nutrient concentrations at 120 m occur during the 1998 La Niña. During the 1997–1998 ENSO, nutrient concentrations start to increase at the end of the negative SOI phase.

Simulated nitrate concentrations are particularly low during the three El Niño periods (1991, 1994, and 1997, Fig. 7A) and decrease below 2 µg l^{-1} during June–December 1997. The highest nitrate concentrations occur in mid-1998 in association with the 1998 La Niña. Ammonium is generally depleted (<0.1 µmol l^{-1}) within the mixed layer during most of the decade (Fig. 7B). The ammonium concentrations reach maximum values during the last 4 months of the negative SOI phase (March 1992, June 1993, March 1995, and February 1998). Ammonium concentration is directly linked to production, after a high production period ammonium concentrations increase due to recycling of previously taken up nitrogen.

Similar to ammonium, iron is also depleted in the mixed layer (<0.03 nmol l^{-1}). Simulated iron concentrations are almost completely depleted within the whole water column during the three El Niño periods (1991, 1994, and 1997). High iron values coincide with both high nitrate and high ammonium values. For example, at the beginning of 1998 an iron maximum (0.25 nmol l^{-1}), similar to ammonium, occurs around 80 m. The highest iron concentrations (0.3 nmol l^{-1})

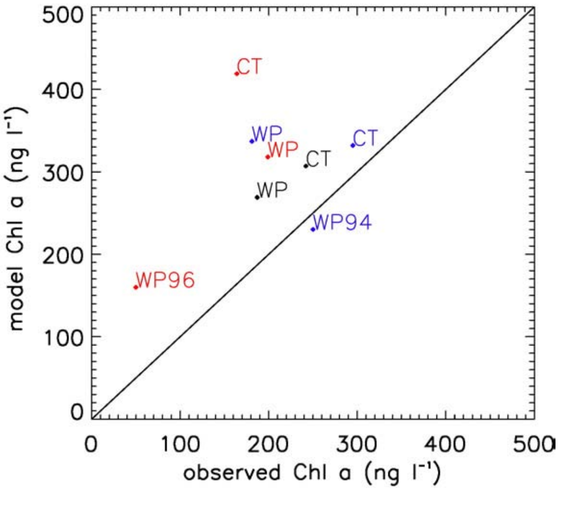

Fig. 6. Comparison of simulated chlorophyll *a* with observed chlorophyll *a* values of sum of all five algal groups. Black symbols show comparison of average values derived from Sea-viewing Wide Field of view Sensor (SeaWiFS) at 0°N, 140°W (CT) and 0°N, 165°E (WP) with corresponding simulated values. The SeaWiFS data set begins in Fall 1997 and continues until the beginning of 1999. The blue and red symbols indicate comparisons during the cold and warm phases of ENSO, respectively. WP94 and WP96 correspond to comparisons during 1994 FLUPAC and 1996 Zonal Flux cruses.

Please cite this article as: Salihoglu, B., Modeling the effect of ENSO on the lower trophic level ecosystem of the Cold Tongue and the Warm Pool regions in the equatorial Pacific, Journal of Marine Systems (2009), doi:10.1016/j.jmarsys.2008.12.004

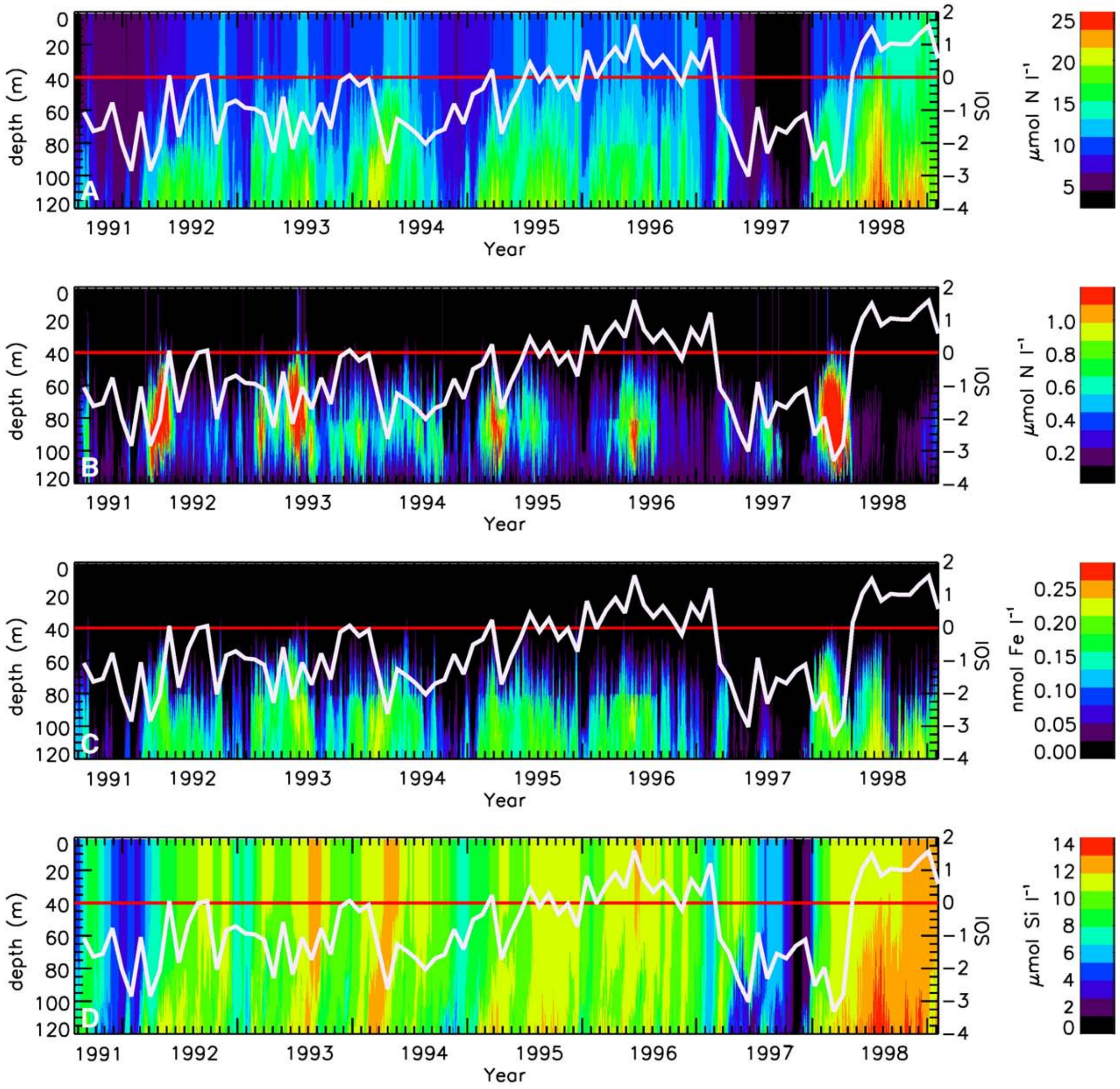

Fig. 7. Simulated depth-time distributions of the concentrations of (A) nitrate, (B) ammonium, (C) iron, and (D) silicate in the Cold Tongue. The SOI is shown (white line) relative to the zero SOI (red line).

occur at 120 m in mid-1998, similar to the nitrate concentrations. Iron concentrations are controlled by inputs at 120 m especially from the EUC and by surface iron deposition as well as by remineralization within the water column. Thus, the simulated vertical iron distributions suggest that the vertical iron distributions show characteristics of both new-(nitrate) and recycled-nitrogen (ammonium).

The simulated silicate distribution follows a pattern similar to nitrate (Fig. 7D). Simulated silicate concentrations are low during the three El Niño periods, although concentrations are never depleted during the 1991 and 1994 El Niños. Contrary to nitrate, silicate is completely depleted (~0 µg l^{-1}) in the upper 100 m during the 1997 El Niño. The highest silicate concentrations also occur during mid-1998, associated with the 1998 La Niña.

4.1.3.1. Impact of time variable iron deposition on primary production. Iron deposition values are obtained from a model (Ginoux et al., 2001) and are not validated for the region, however, these estimates are useful to test model sensitivity to variability in atmospheric iron flux. A mean constant aeolian iron deposition instead of a time variable iron deposition (Fig. 2C) does not change the integrated annual primary production in the Cold Tongue region. The maximum difference in primary production between the two model runs is 0.5 µmol C l^{-1} d^{-1} (Fig. 8A). This small difference indicates that the time variability in aeolian iron deposition is not strong enough to significantly alter the annual integrated production of phytoplankton blooms in the Cold Tongue region (Fig. 3).

The effect of a time invariant iron deposition is shown best by the difference in primary production obtained from the

Please cite this article as: Salihoglu, B., Modeling the effect of ENSO on the lower trophic level ecosystem of the Cold Tongue and the Warm Pool regions in the equatorial Pacific, Journal of Marine Systems (2009), doi:10.1016/j.jmarsys.2008.12.004

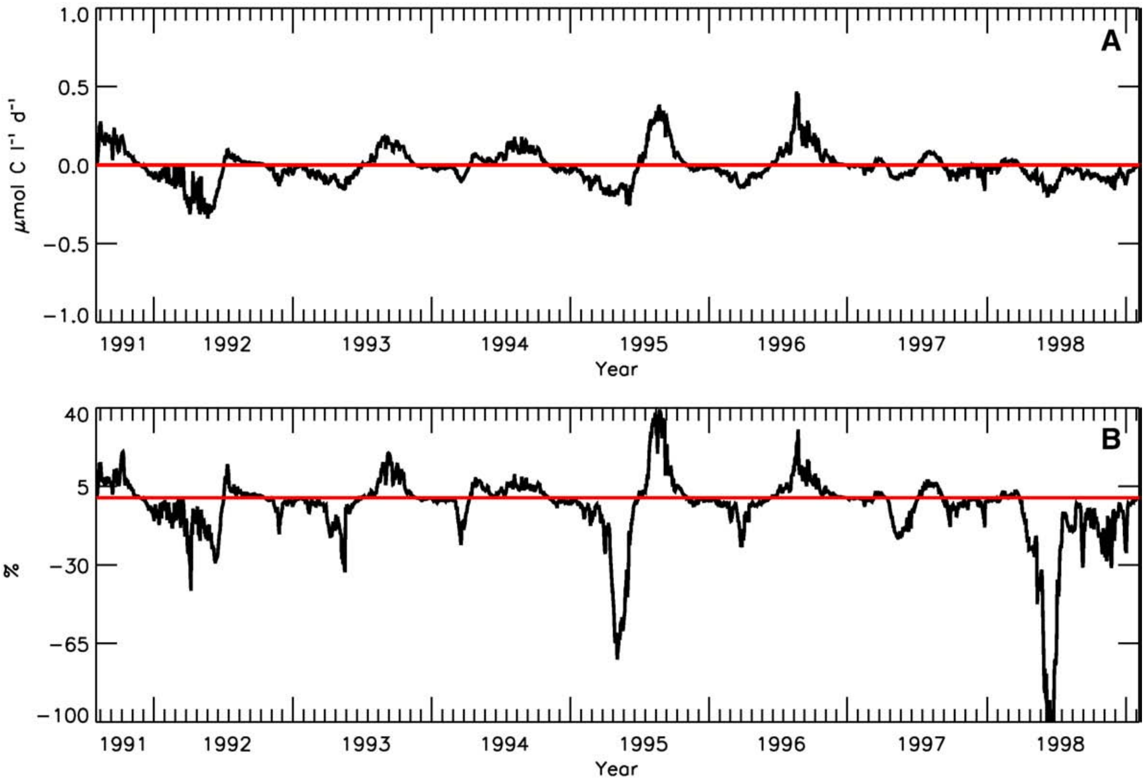

Fig. 8. Change in primary production in the Cold Tongue mixed layer in response to setting the aeolian iron deposition to a mean value of 0.013 nmol l^{-1} h^{-1}. Actual (A) and percent (%) (B) difference between the reference simulation and the simulation in which a constant (time invariant) aeolian iron deposition is used. Red lines in both panels indicate the zero difference between two model runs.

reference simulation and the constant iron source simulation (Fig. 8A). The largest difference occurs during years 1995 and 1996 when iron deposition is particularly high (Fig. 2C). However the percent difference in primary production between the two models runs does not follow this pattern (Fig. 8B). Variable iron deposition increases primary production up to 40% during year 1995 and also decreases primary production up to 100% in 1998 (Fig. 8B). During these periods the actual simulated primary production is low (Fig. 3). Thus, even a small net decrease in primary production relative to other periods results in a high percentage decrease for 1995 and 1998 (Fig. 8B). The large percent change due to variations in the iron input source suggests that aeolian iron deposition is responsible for a major part of phytoplankton primary production during these seasons.

4.2. Diel variations in mixed layer depth

The deepest seasonal mixed layers (~120 m) occur during El Niño periods (Fig. 2B) and the shallowest (10–30 m) occur during La Niña conditions in the Cold Tongue region. Superimposed on the seasonal change is strong diurnal variability in

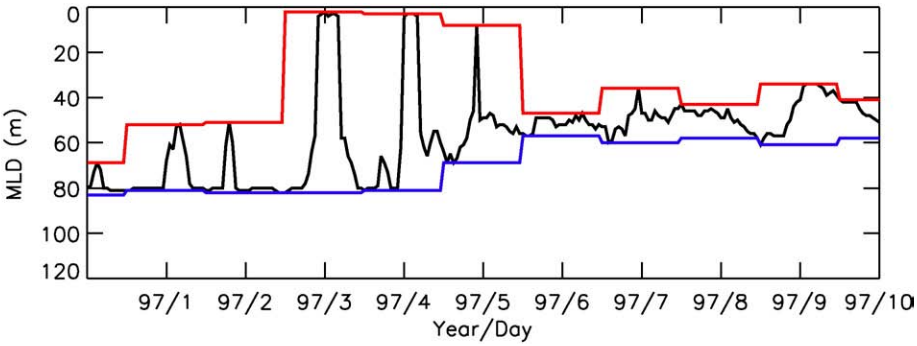

Fig. 9. Mixed layer depth (MLD) during the first 10 days of year 1997 estimated from temperature measurements from the TAO mooring at 0°N, 140°W. The upper (red) and lower (blue) solid lines indicate the daytime and nighttime mixed layer depths, respectively.

Please cite this article as: Salihoglu, B., Modeling the effect of ENSO on the lower trophic level ecosystem of the Cold Tongue and the Warm Pool regions in the equatorial Pacific, Journal of Marine Systems (2009), doi:10.1016/j.jmarsys.2008.12.004

mixed layer depth (Fig. 9), which is caused by the diurnal heating of the surface waters. Heating stratifies the surface waters during the day, and convective cooling mixes the water at night (Price et al., 1986; Schudlich and Price, 1992; Anis and Moum, 1994). D'Asaro et al. (1996) showed that the depth of the active mixing varies between day and night. Thus, as a sensitivity study the influence of a diurnally varying mixed layer depth (MLD) on the distribution of the model state variables is tested.

In the equatorial Pacific Ocean variations in depth of the diel mixed layer using the 1°C difference from the SST criterion, are up to 110 m during El Niño periods, but are seldom over 25 m during La Niñas. The strongest diel fluctuations in the mixed layer depth are estimated for the 1997–1998 El Niño, which are as great as 110 m.

Simulations that use a mixed layer depth that undergoes a diurnal deepening and shallowing show that this process can significantly affect the distribution of chlorophyll *a*, and influence primary production by pumping nutrients upward and by controlling light levels experienced by phytoplankton (not shown). Many of the biochemical pools included in the lower trophic level model have strong gradients in the upper 100 m of the ocean and high frequency oscillations in the depth of mixing can be important in enhancing vertical exchange in surface waters. Those components of the lower trophic level ecosystem with high surface concentrations (i.e. phytoplankton and zooplankton) are mixed downwards, while those with concentrations that increase with depth (i.e. nutrients) are pumped upward.

Inclusion of a diurnally-varying mixed layer depth increases the simulated annual primary production by 9% compared to using only a daytime (minimum) mixed layer depth. The night-time (maximum) mixed layer depth produces only a 1.4% increase in annual primary production, relative to the value obtained using a variable mixed layer depth.

4.3. Comparison of two ecosystems, Cold Tongue versus Warm Pool

4.3.1. Warm Pool environmental time series

The effect of the SOI on the Warm Pool differs from that observed for the Cold Tongue region. The water temperatures at 120 m begin cooling right after the SOI switches to the negative phase (El Niño) and continue to decrease during the negative phase (Fig. 10A) unlike the Cold Tongue where El Niño conditions correspond to anomalously warm waters. During the positive phases of SOI (La Niña) water temperatures in the Warm Pool region are warmer than usual (Fig. 10A).

The estimated mean mixed layer depths in the Warm Pool region are deeper than those estimated for the Cold Tongue

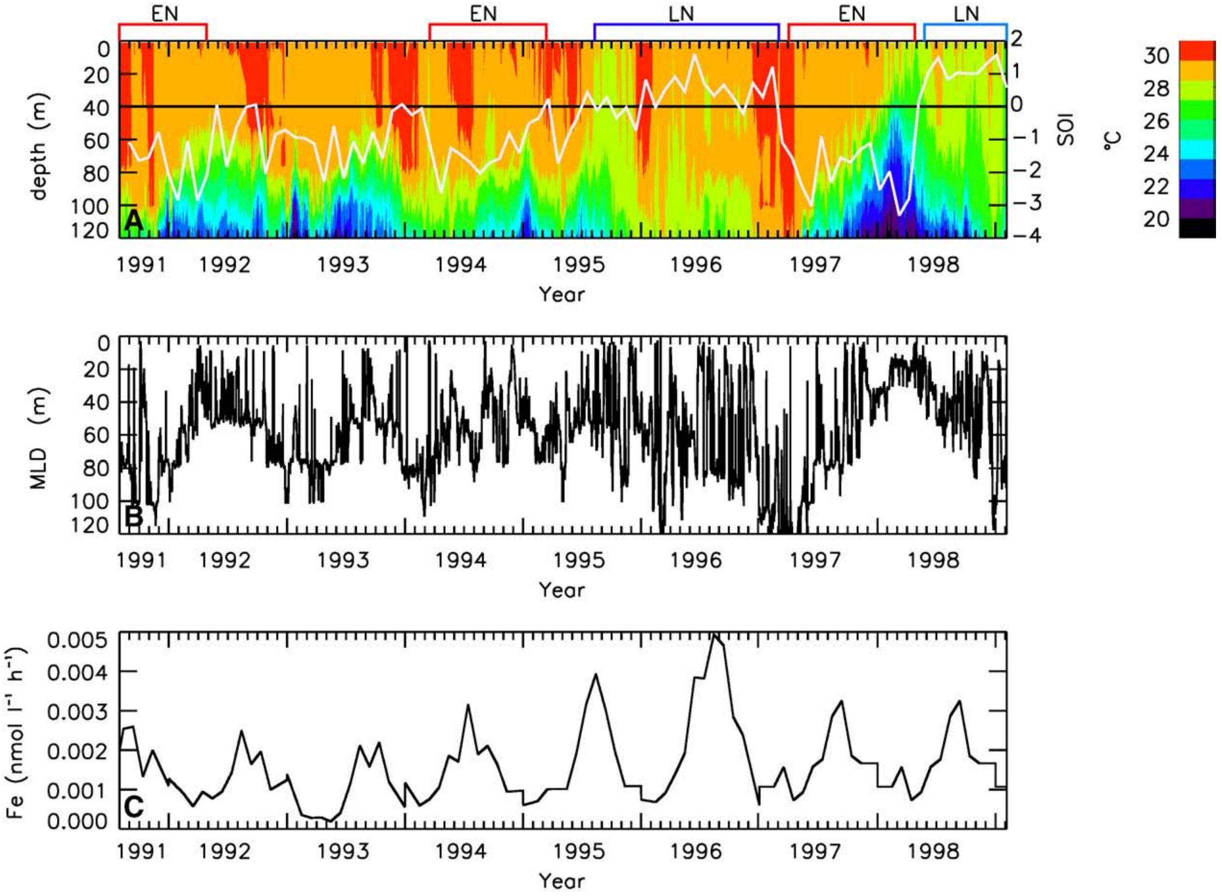

Fig. 10. Depth-time distribution of (A) temperature, (B) estimated mixed layer depth (MLD) and, (C) aeolian iron flux (Ginoux et al., 2001) for 1991 to 1999 for the Warm Pool (0°N, 165°E) region. The temperature and MLD are from the TAO mooring at 0°N, 165°E. The SOI is shown in panel A (white line) relative to the zero SOI (black line). The time periods of El Niños (EN, red) and La Niñas (LN, blue) are shown.

Please cite this article as: Salihoglu, B., Modeling the effect of ENSO on the lower trophic level ecosystem of the Cold Tongue and the Warm Pool regions in the equatorial Pacific, Journal of Marine Systems (2009), doi:10.1016/j.jmarsys.2008.12.004

region (average depth of 59 versus 44 m). Unlike in the Cold Tongue region, the estimated mixed layer depths associated with the La Niña episodes are deeper than those that occur during the El Niño events in the Warm Pool (Fig. 10B). During the El Niño periods of 1994 and 1997 mixed layer depths stay particularly shallow (~30 m). The mixed layer depth extends to 120 m at the beginning of the 1997 El Niño and shoals afterwards as the event develops.

The aeolian iron flux obtained from Ginoux et al. (2001) for the Warm Pool indicates a strong annual variability in iron deposition similar to what is obtained for the Cold Tongue region (Fig. 10C). The least iron deposition occurs during February–April and the highest during August–October. Year 1996 corresponds to a high dust deposition period.

The annual cycle of irradiance in the Warm Pool is similar to the Cold Tongue, and the variability in annual irradiance is low in both regions (±50 µmol quanta m^2 s^{-1}). The general cloud cover is higher in the Warm Pool compared to the Cold Tongue. There is no linear correlation between the SOI and the cloud cover in the Warm Pool. The start of the high cloud cover occurs towards the end of the positive phase of SOI and continues as the SOI switches to negative (not shown, cf. Salihoglu, 2005).

4.3.2. Phytoplankton

The simulated annual integrated primary production in the Warm Pool is 20% lower than that obtained for the Cold Tongue. However, there is only a small difference (5%) in integrated algal biomass between the two regions, although the distribution of each algal group biomass shows distinct differences between the two regions.

The simulated depth-time distributions of the five algae groups at 0°N, 165°E for 1991–1999 (not shown) indicate that in the Warm Pool the highest algal group biomass concentrations occur during the El Niño phases contrary to what happens in the Cold Tongue region. Algal group 4 dominates the phytoplankton community assemblage in the Warm Pool, but this dominance is not continuous as it is in the Cold Tongue. During cold periods algal group 4 becomes dominant and during warm periods the biomass of *Prochlorococcus* spp. (algal group 1 + 2) is as high as that of algal group 4.

Simulations indicate that the deep chlorophyll maximum in the Warm Pool (Fig. 11) is in general deeper than the deep chlorophyll maximum in the Cold Tongue (Fig. 5) (~50 m versus ~65 m). The surface chlorophyll *a* values in the Warm Pool are low, with a mean concentration of 0.25 µg l^{-1}. During the warm periods chlorophyll *a* concentrations are below 0.2 µg l^{-1} and increase to 0.4 µg l^{-1} during the cold periods. The highest simulated chlorophyll *a* values (1.1 µg l^{-1}) are at 40 m during 1995, which corresponds to the end of the 1994–1995 El Niño when cold waters reach the surface (Fig. 10A). During this period the highest surface values are 0.8 µg l^{-1}.

The comparison of simulated chlorophyll *a* versus SeaWiFS chlorophyll *a* (Fig. 6) shows that the simulated biomass during both El Niño and La Niña conditions overestimate the observed values. The underlying processes that control the phytoplankton dynamics given in this section is explained in Section 5.1.3.

4.3.3. Nutrients

The simulated distributions of the four nutrients in the upper 120 m in the Warm Pool at 0°N, 165°E are low during La Niña periods and high during El Niño periods (Fig. 12A–D). The highest nutrient concentrations occur during the negative phases of SOI and the lowest concentrations occur during La Niña (positive SOI) periods.

The simulated distributions indicate that surface nitrate levels in the Warm Pool are much lower (annual mean of 1.2 µmol l^{-1}, Fig. 12A) than those in the Cold Tongue (annual mean of 8.9 µmol l^{-1}, Fig. 7A). The highest nitrate levels occur in the Warm Pool during the 1997–1998 and 1991–1993 El Niños. During the rest of the decade nitrate is depleted (<1 µmol l^{-1}) in the surface waters.

In general ammonium concentrations are low (<0.1 µmol l^{-1}) above 40 m. There is a strong (~1 µmol l^{-1}) ammonium maximum centered at ~80 m (Fig. 12B), which persists throughout the 1990s, except for the 1995–1996 La Niña period. The strength of this ammonium maximum differs from that seen in the Cold Tongue simulations where ammonium maxima values rarely reached 1 µmol l^{-1} (Fig. 7B).

The Warm Pool simulations show that this region is also iron depleted (Fig. 12C), similar to what is found for the Cold Tongue (Fig. 7C). The iron concentrations are also very low above 40 m (<0.1 nmol l^{-1}), although the mean surface iron concentration is more than double the mean iron concentration in the Cold Tongue (0.07 versus 0.03 nmol l^{-1}, respectively). This shows that iron can be depleted through uptake to a greater extend in the Cold Tongue.

The simulated silicate concentrations in the Warm Pool (Fig. 12D) are lower than those obtained for the Cold Tongue (Fig. 7D). However, silicate concentrations in the Warm Pool are never depleted, except at the beginning of 1997 (~0.5 µg l^{-1}), which corresponds to the end of the 1995–1996 La Niña. For a persistent negative SOI, which corresponds to upwelling of cold waters at 120 m and surface stratification (Fig. 10A), silicate tends to accumulate in the mixed layer. During the 1991–1993

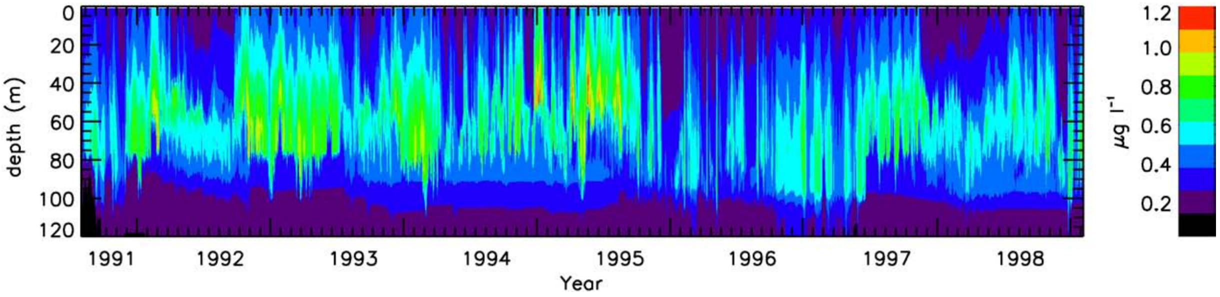

Fig. 11. Simulated depth-time distributions of chlorophyll *a* (µg l) obtained from the sum of all five algal groups in the Warm Pool at 0°N, 165°E for 1991–1999.

Please cite this article as: Salihoglu, B., Modeling the effect of ENSO on the lower trophic level ecosystem of the Cold Tongue and the Warm Pool regions in the equatorial Pacific, Journal of Marine Systems (2009), doi:10.1016/j.jmarsys.2008.12.004

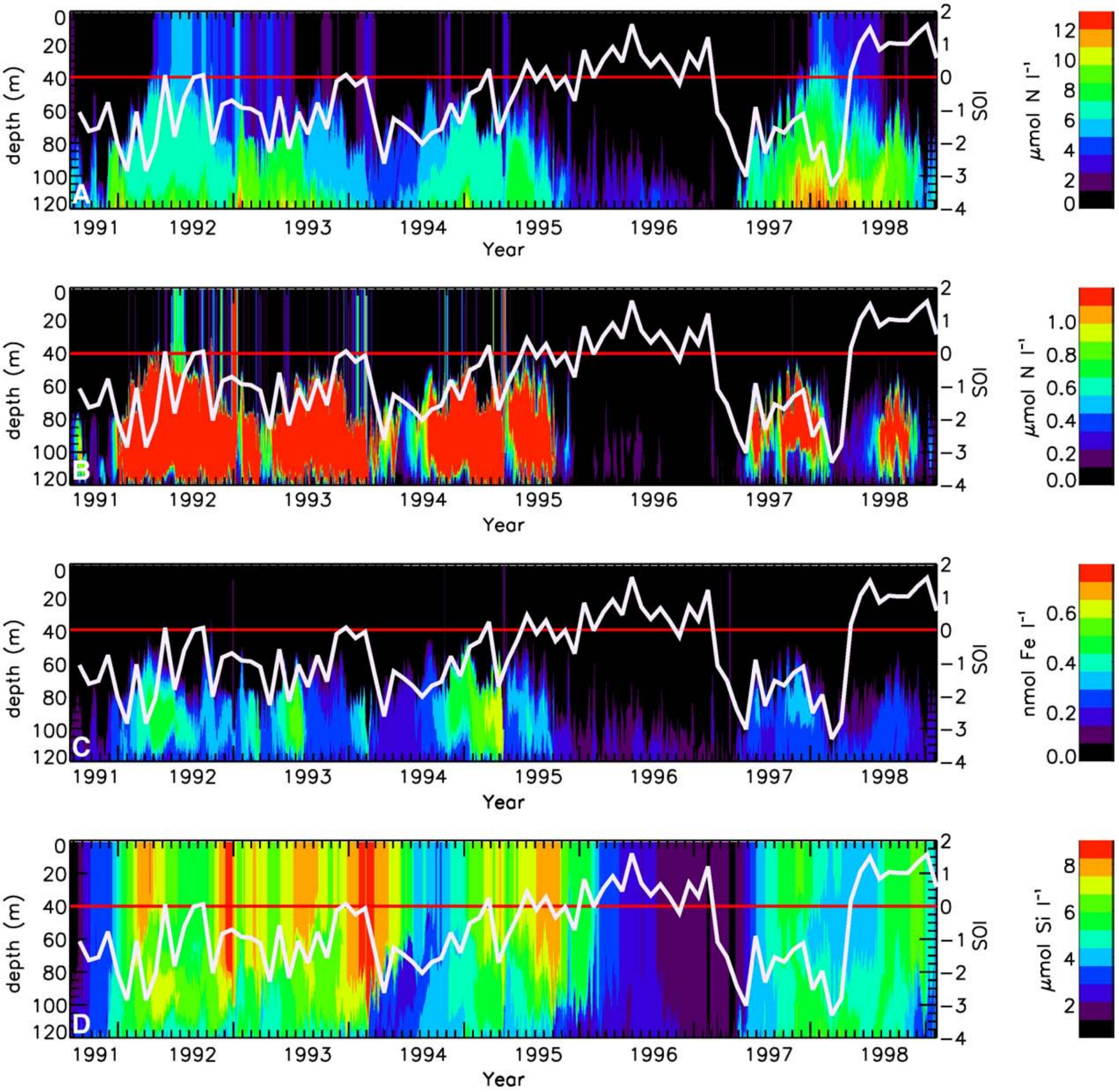

Fig. 12. Simulated depth-time distributions of the concentrations of (A) nitrate, (B) ammonium, (C) iron, and (D) silicate in the Warm Pool. The SOI is shown (white line) relative to the zero SOI (red line).

El Niño when these conditions prevailed in the Warm Pool region, the simulated silicate concentrations are above 8 nmol l^{-1} in the mixed layer. During this period silicate that is introduced into the euphotic zone stays in the stratified water column where high water temperatures enhances its recycling.

4.3.4. Model-data comparison

The lower trophic level ecosystem model is not explicitly developed for the Warm Pool, and as a result the Warm Pool simulations provide additional model comparison studies. The simulated distributions are compared with measurements made during the 1994 FLUPAC and 1996 Zonal Flux cruises (cf. Section 2) that took place in the Warm Pool to provide an assessment of the general applicability of the model structure.

Overall, the simulated nutrient and primary production values compare well with measurements (Table 1), the measurements have poor space and time resolution relative to the simulated values and as a result may not be directly comparable to the simulated values. Also, it is shown by Aufdenkampe and Murray (2002) that nutrient, new and primary production values for a particular cruise depends on the type of temporal and spatial variability that is encountered during the cruise. It is generally not possible to include this variability in the model forcing fields. The observed and simulated surface concentrations of nitrate and ammonium compare well during the 1994 FLUPAC cruise, which corresponds to an El Niño period. The observed surface silicate concentrations are lower than the simulated values during this time. The model overestimates the 120-m integrated

Please cite this article as: Salihoglu, B., Modeling the effect of ENSO on the lower trophic level ecosystem of the Cold Tongue and the Warm Pool regions in the equatorial Pacific, Journal of Marine Systems (2009), doi:10.1016/j.jmarsys.2008.12.004

Table 1
Comparison of simulated nitrate (NO_3^-), ammonium (NH_4^+), silicate ($Si(OH)_4$), and primary production (PP) values with their corresponding values measured during the 1994 FLUPAC and 1996 Zonal Flux cruises in the Warm Pool at 0°N, 165°E

	Unit	Time	Observed	Modeled
NO_3^- surface (0–30 m)	$\mu mol\ l^{-1}$	29/9/1994	0.003	0.002
NO_3^- total (0–120 m)	$mmol\ m^{-2}$	29/9/1994	172	299
NO_3^- surface (0–30 m)	$\mu mol\ l^{-1}$	22/4/1996	2.61	0.82
NO_3^- total (0–120 m)	$mmol\ m^{-2}$	22/4/1996	313	265
NH_4^+ surface (0–30 m)	$\mu mol\ l^{-1}$	29/9/1994	0.01	0.01
NH_4^+ total (0–120 m)	$mmol\ m^{-2}$	29/9/1994	3.6	28
NH_4^+ surface (0–30 m)	$\mu mol\ l^{-1}$	22/4/1996	0.9	0.01
NH_4^+ total (0–120 m)	$mmol\ m^{-2}$	22/4/1996	94.4	11
$Si(OH)_4$ surface (0–30 m)	$\mu mol\ l^{-1}$	29/9/1994	1.7	3.5
$Si(OH)_4$ total (0–120 m)	$mmol\ m^{-2}$	29/9/1994	325	470
$Si(OH)_4$ surface (0–30 m)	$\mu mol\ l^{-1}$	22/4/1996	4.75	3.14
$Si(OH)_4$ total (0–120 m)	$mmol\ m^{-2}$	22/4/1996	480	334
PP surface (0–30 m)	$\mu mol\ l^{-1}\ d^{-1}$	3/10/1994	0.85	2
PP total (0–120 m)	$mmol\ m^{-2}\ d^{-1}$	3/10/1994	74	95.57
PP surface (0–30 m)	$\mu mol\ l^{-1}\ d^{-1}$	22/4/1996	1.5	0.3
PP total (0–120 m)	$mmol\ m^{-2}\ d^{-1}$	22/4/1996	93.8	47

nutrient values compared to those obtained from nutrient measurements made during the 1994 FLUPAC cruise. The model results underestimate both the surface and integrated nutrient concentrations compared to measured values from the 1996 Zonal Flux cruise, which corresponds to the 1995–1996 La Niña period. As a result of this mismatch in the nutrient concentrations, the simulated primary production values for 1994 overestimate the values measured in 1994 and underestimate the values measured in 1996. This can also be seen in the chlorophyll *a* fields (Fig. 6). The comparison of simulated chlorophyll *a* versus SeaWiFS chlorophyll *a* (Fig. 6) shows that the simulated biomass during both El Niño and La Niña conditions overestimate the observed values. The underlying processes that control the phytoplankton dynamics given in this section are explained in Section 5.1.3.

No direct iron measurements are available for 0°N, 165°E. However, some historical data for this region are available (Johnson et al., 2002). Comparisons of the simulated iron concentrations to the historical iron measurements show that the simulated values are realistic in that iron levels above 80 m are less than 0.1 nmol l^{-1} (Fig. 12C). Observed iron concentrations at 120 m are about 0.2 nmol l^{-1}, which is also consistent with simulated concentrations.

4.3.5. Iron dynamics

To test the effect of iron on limiting production in the Warm Pool a simulation is done using the iron-temperature relationship developed for the Cold Tongue (Eq. (2)). The resultant annual primary production values are about 50% of those obtained for the Cold Tongue region (27,022 versus 14,338 mmol C $m^{-2}\ yr^{-1}$). The iron-temperature relationship developed for the Warm Pool (Eq. (6)) results in an increase of annual primary production by almost 75% in comparison to using Eq. 2, but this value is still 22% lower than the annual primary production estimated for the Cold Tongue.

The pattern of aeolian iron deposition differs between the two regions (Fig. 2C versus 10C), but the mean deposition in both regions is almost the same (~0.038 nmol $l^{-1}\ h^{-1}$). The simulations indicate that the effect of aeolian iron deposition on the Warm Pool ecosystem is somewhat stronger than its

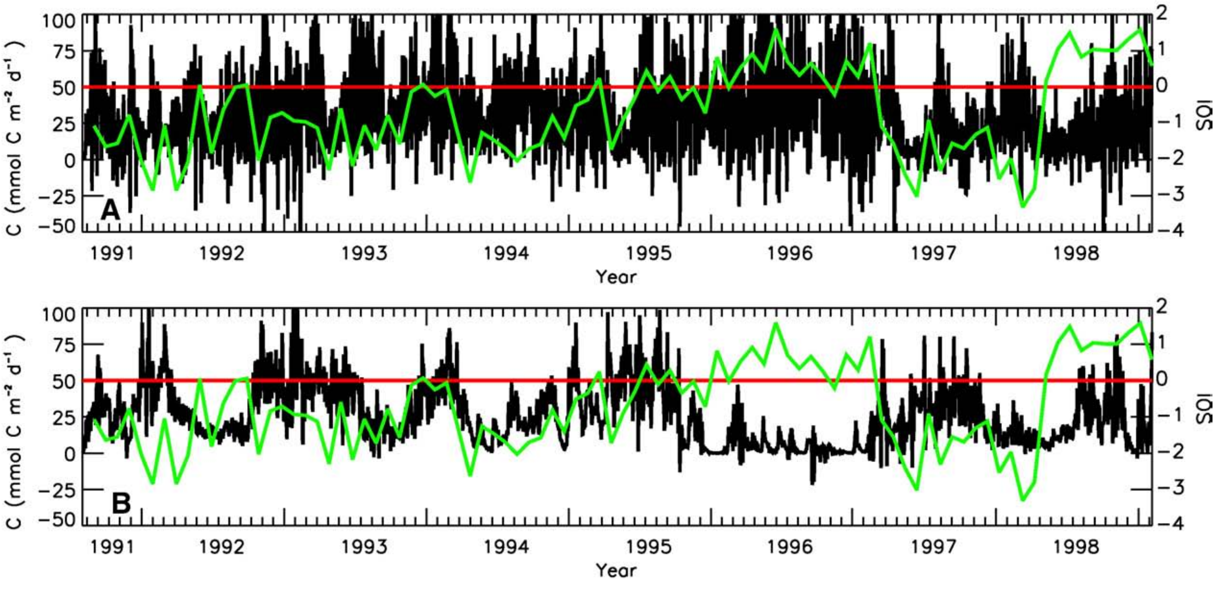

Fig. 13. Simulated time distribution of particulate carbon export fluxes at 120 m in the Cold Tongue (A) and in the Warm Pool (B). The SOI is shown (green line) relative to the zero SOI (red line).

Please cite this article as: Salihoglu, B., Modeling the effect of ENSO on the lower trophic level ecosystem of the Cold Tongue and the Warm Pool regions in the equatorial Pacific, Journal of Marine Systems (2009), doi:10.1016/j.jmarsys.2008.12.004

effect on the Cold Tongue ecosystem. Elimination of iron via aeolian deposition decreases the annual primary production of the Warm Pool by 20% and that of the Cold Tongue by 17%. Algal group 4 in the Warm Pool ecosystem is most affected by removal of aeolian deposition, showing a 24% decrease in annual primary production.

The simulated iron remineralization has a substantial influence on the Warm Pool carbon production, accounting for 50% of the annual primary production. This is higher than the 40% annual primary production in the Cold Tongue that is supported by iron remineralization.

4.3.6. Export production

The simulated annual carbon fluxes at the base of the euphotic zone (120 m) in the Warm Pool are 22% lower than the equivalent carbon flux calculated for the Cold Tongue. These results are consistent with observations, which showed that the mean particulate organic carbon (POC) flux in the Warm Pool is ~15% lower than that in the Cold Tongue region (Dunne et al., 2000).

In the Cold Tongue region during the cold (positive) phases of SOI the carbon export is high compared to the warm (negative) phases of SOI, except at the beginning of 1997, when high export production is seen in the simulated time series (Fig. 13A). In contrast, there is no apparent correlation between export carbon production and the SOI in the Warm Pool (Fig. 13B). The periods of highest simulated export carbon production coincide with the negative phases of SOI. During 1996, when the SOI is persistently positive, the export carbon production in the Warm Pool is near zero.

In both regions export carbon production values are variable. For example, in the Cold Tongue (Fig. 13A) the export carbon fluxes are ~3 times higher during the 1995–1996 La Niña than during the 1994 El Niño. In the Warm Pool low frequency variability dominates the simulated export carbon flux (Fig. 13B); whereas, the Cold Tongue export carbon flux shows more influence from high frequency motions (Fig. 13A). This implicates that the impact of physical variability on biology is greater in the Cold Tongue than in the Warm Pool as suggested by Stoens et al. (1999). In the Warm Pool, the difference in the simulated export carbon flux between the cold and warm phases can increase by a factor of five.

5. Discussion

5.1. Effect of ENSO on the Cold Tongue and the Warm Pool ecosystems

5.1.1. Cold Tongue

The rate of primary production in the Cold Tongue is directly related to the phase of the SOI, with decreased production associated with decreasing and negative SOI values, which occur during El Niños (Fig. 3). These periods correspond to low nutrient concentrations at the base of the euphotic zone (Fig. 7A–D), because the EUC, which pumps nutrient-rich (e.g., iron) cold waters into surface waters, is weaker and deeper during El Niños (Barber et al., 1996).

During the mature phases of La Niñas, the simulated algal primary production and biomass is not as high compared to the biomass and primary production at the beginning of La Niñas. Although during the mature phases of La Niñas the upwelling of nutrients is stronger (Fig. 7A–D), the mixed layer depths are much shallower due to shallow thermocline depths and the water temperatures are lower (Fig. 2A and B). The shallow mixed layer depths result in reduced mixing of nutrient rich waters into the surface waters and low temperatures result in reduced growth rates and reduced recycling of iron and ammonium.

Based on simulations of the lower trophic levels of the Cold Tongue, Leonard et al. (1999) suggested that primary production in this region can show considerable interannual variability, with 50% more primary production occurring during non-ENSO conditions compared to El Niño conditions. The simulated primary production estimates from this study agree with this conclusion and further suggest a 3-fold short-term variability in primary production between the end of the El Niño and beginning of La Niña.

Recent studies showed that primary production in the Cold Tongue is affected by TIWs (Chavez et al., 1999; Friedrichs and Hofmann, 2001) and Kelvin waves (Chavez et al., 1998; Murtugudde et al., 1999; Radenac et al., 2001). The simulated carbon export dynamics obtained from 0°N, 140°W (Fig. 13A) is enhanced during the periods where observed TIWs are present and diminished when Kelvin waves occur, which occur during the latter part of 1992 and the beginning of 1997, respectively. The simulated changes in carbon export productions in response to environmental structure variability are consistent with the observations by Dunne et al. (2000). During the second part of 1992 and the beginning of 1997, the simulated iron inputs in the Cold Tongue at 120 m (from the EUC) are closely linked to the passage of TIWs and Kelvin waves (Fig. 7C), which agrees with previous studies (Barber et al., 1996; Foley et al., 1997; Friedrichs and Hofmann, 2001; Radenac et al., 2001). Recently, Gorgues et al. (2005) suggested that TIWs may reduce iron concentrations, thus the chlorophyll and new production at the equator. They claimed that TIW-induced horizontal advection exports iron-depleted water to the equator. Because my model does not explicitly include horizontal dynamics, it is not possible to test this hypothesis.

5.1.2. Effect of diurnal mixing in the Cold Tongue

Variability in the mixed layer and diel changes in mixed layer depth significantly affect the simulated distribution of chlorophyll *a* and influence primary production rates by pumping nutrients upward and controlling the light levels experienced by phytoplankton. Many of the biochemical variables included in the lower trophic level model have strong gradients in the upper 100 m of the ocean. Thus, oscillations in the depth of mixing is an important component of vertical exchange in the surface waters. Biochemical quantities with high surface concentrations (e.g., phytoplankton) are mixed downward, those with concentrations that increase with depth (e.g., nutrients) are pumped upwards.

The simulated nutrient distributions reflect observations that show that heating stratifies the surface waters at 0°N, 140°W during the day and convective cooling mixes the water at night (Gardner et al., 1995). Night-time deepening entrains nutrient-rich waters into the mixed layer and day-time shoaling of the mixed layer confines these nutrient-rich waters to high-light levels that accelerate biological production.

Please cite this article as: Salihoglu, B., Modeling the effect of ENSO on the lower trophic level ecosystem of the Cold Tongue and the Warm Pool regions in the equatorial Pacific, Journal of Marine Systems (2009), doi:10.1016/j.jmarsys.2008.12.004

Denman and Marra (1986) showed that large variations in the depth to which phytoplankton are mixed can affect their growth rates because of differences in the light field within the mixed layer. Simulation results suggest that during the night, the phytoplankton biomass is diluted as the mixed layer depth increases, which results in intrusion of nutrients into the surface waters. However, during the day the mixed layer depth shoals and production increases as light levels increase, resulting in an increase in biomass. This diurnal dilution allows the phytoplankton to take advantage of high nutrients below the day-time mixed layer. Thus, model results show that annual primary production is 9% higher when the diurnal mixed layer variability is included compared to using only a day-time (minimum) mixed layer depth. However, using the night-time (maximum) mixed layer depth produces a 1.4% increase in annual primary production, which results from intrusion of nutrients into the surface waters during the day. This indicates that the shallower mixed layer depths during the day should not have a big influence on the light-dependent growth of phytoplankton in the eastern equatorial Pacific.

The effect of the variability of the mixed layer depth on particle export out of the euphotic zone has long been discussed. Kerr and Kuiper (1997) suggested that if the mixed layer depth in the ocean does not show variability and the particles are assumed to sink at a constant rate, there would be an equal flux of particles out of the mixed layer under steady state conditions regardless of the presence or absence of convective mixing. However, the variability in the mixed layer in the open ocean can potentially affect the export of particles from the mixed layer. Gardner et al. (1995) argued that the effect of diel changes in the mixed layer depth may enhance the carbon removal out of the euphotic zone. Diel changes in the mixed layer depth can isolate particles from mixing in the surface waters as the mixed layer shoal during the day. This would allow the particles below the mixed layer depth to settle at their sinking speed. This would be especially effective for fast sinking particles which can settle deeper than the mixed layer depth of the following evening, thereby allowing particles to be pumped from the surface waters. Contrary to this, Alldredge et al. (1987) argued that a night-time increase in the intensity of mixing would redistribute the particulate material within the mixed layer, thus prolonging their residence time in the euphotic zone. However, the simulation results show that the increase in carbon export from the euphotic zone for a diurnally varying mixed layer relative to the value obtained from simulations using the day-time (minimum) mixed layer depth is identical to the increase in carbon production between two simulations. Thus, increases in carbon export are primarily a function of primary production and are not greatly affected by the downward transport of particulate matter due to the diurnal deepening of the mixed layer or by the redistribution of particulate matter throughout the mixed layer. It is possible that pumping of particulate material out of the euphotic zone and redistribution of particulate material throughout the mixed layer are counterbalanced.

5.1.3. Warm Pool

The environmental conditions in the Warm Pool differ considerably from those in the Cold Tongue. The upper ocean in the Warm Pool is highly stratified and water temperatures from the surface to 120 m are in general warmer than those in the Cold Tongue. The strongest cooling occurred during the 1997–1998 El Niño (Fig. 10A).

The simulated nutrient distributions show increased levels at the base of the euphotic zone in the Warm Pool during El Niño conditions (Fig. 12A–D). This arises because the EUC, which pumps the nutrient-rich cold waters into the surface, shoals in the eastern Pacific during El Niños (Barber et al., 1996; Le Borgne et al., 2002). As a result the highest primary production and algal biomass concentrations in the Warm Pool occur during El Niño phases instead of during La Niña phases; as occurs in the Cold Tongue. The highest simulated chlorophyll *a* concentrations (Fig. 11) occur during the 1995 El Niño because cold nutrient-rich waters reach to the surface and the mixed layer depth extends to 90 m (Fig. 2B). The maxima in chlorophyll *a* coincides with the deepening of the mixed layer depth. During the 1997 El Niño cold waters also reach the surface but during this period the estimated mixed layer depths are very shallow (~20 m) therefore the simulated primary production is not as high as during the 1995 El Niño.

Le Borgne et al. (2002) suggested that while iron limits primary production in the Cold Tongue, macronutrients control the primary production in the Warm Pool region. The simulations from the Cold Tongue and the Warm Pool regions show that the primary production and carbon export flux in the Cold Tongue is higher than the Warm Pool, although the iron levels are much higher in the Warm Pool. This suggests that in the Cold Tongue the high rates of primary production relative to the Warm Pool is not due to iron but it is the effect of high macronutrient concentrations in the region. Model results further suggest that the primary production is mainly controlled by iron in the Cold Tongue; whereas, the combined effects of macronutrients and iron control the Warm Pool primary productivity. This result is supported by a recent study by Behrenfeld et al. (2006) which hypothesized that 165°E on the equator is part of a physiological regime that is iron limited and has low macronutrients whereas 140°W belongs to a regime that is iron limited but has high macronutrients.

The phytoplankton assemblage in the Warm Pool consists of the normal background levels of small phytoplankton (*Prochlorococcus* spp., *Synechococcus*). The larger phytoplankton become abundant during periods of upwelling, which introduces nutrients to the surface. This produces algal biomass, mean organism size, and export fluxes that are greater than what occurs in the normally nutrient-depleted waters of the Warm Pool. However, the difference in annual simulated carbon export between the Warm Pool and Cold Tongue is small (22% higher in the Cold Tongue) because of the limitation of primary production in the upwelling zone by iron and, possibly by other nutrients. These results are consistent with observations (Le Borgne et al., 2002).

However, the nutrient, chlorophyll *a* and primary production observations obtained during the FLUPAC and Zonal Flux cruises at specific days show mismatches with simulated distributions (Section 4.3.4). The October 1994 FLUPAC cruises took place under El Niño conditions and April 1996 Zonal Flux cruises took place under La Niña conditions. During the FLUPAC cruises, the thermocline is elevated in the Warm Pool region and intrusions of nutrient-rich cold waters are

Please cite this article as: Salihoglu, B., Modeling the effect of ENSO on the lower trophic level ecosystem of the Cold Tongue and the Warm Pool regions in the equatorial Pacific, Journal of Marine Systems (2009), doi:10.1016/j.jmarsys.2008.12.004

observed at the bottom of the euphotic zone (Fig. 10A). During the Zonal Flux cruises the thermocline is depressed in the Warm Pool region and nitrate levels are low at 120 m (Dunne et al., 2000). The simulated nutrient concentrations (Fig. 12A, B and D) and primary production rates in the Warm Pool are higher during October 1994 compared to April 1996, however the observations show that the nutrient concentrations and primary production rates are higher during April 1996. The observed depletion of nitrate in the upper 70 m during the 1994 FLUPAC cruises may be produced by the "barrier layer", which is defined as the difference between the thickness of the isothermal layer and the mixed layer (determined by a defined change in density), with the isothermal layer generally being greater than or equal to the mixed layer (Le Borgne et al., 2002). The barrier layer is produced by the difference between the depth of the isohaline and the isothermal layers in the Warm Pool region (Lukas and Lindstrom, 1991; Sprintall and McPhaden, 1994). This feature is not correctly represented by the environmental time series input to the model and its absence may explain some of the discrepancies in simulated and observed quantities.

The high salinity barrier layer that is present between the mixed layer and the thermocline suppresses nutrient fluxes (Le Borgne et al., 2002). The mixed layer depth time series input into the model are estimated from a defined change (1°C) in temperature from the SST (which corresponds to the thickness of the isothermal layer) which may result in mixed layer depths that are deeper than actual depths. Also, the mixed layer in the model is assumed to be homogeneous, an assumption which is not strictly correct (Archer, 1999). Therefore, the mechanism that keeps high nutrient waters from mixing into surface waters under stratified conditions is missing in the model dynamics, allowing nutrients to penetrate into surface waters in the Warm Pool during the warm phases of ENSO.

The simulated iron concentrations indicate that the iron-temperature regression developed for the Warm Pool (Section 4.3.3) gives results consistent with the observations (Johnson et al., 2002). The iron-temperature regression developed for the cold waters at 0°N, 140°W gives low iron concentrations at the base of the euphotic zone, which results in 50% less simulated annual primary production in the Warm Pool relative to the Cold Tongue and accumulation of macronutrients in the surface waters. These results indicate that the iron-temperature relationship undergoes regional variations and that this relationship needs to be developed using *in situ* measurements for the area of interest.

5.2. 1997–1998 El Niño–La Niña

The onset of the 1997 El Niño started with the eastward propagation of an equatorially trapped Kelvin wave (McPhaden, 1999). Observations (Chavez et al., 1998; Strutton and Chavez, 2000) show that the biological response to the Kelvin waves is manifest as a depression in primary production at the beginning of 1997, followed by an increase in primary production to a rate of 100 mmol C m^{-2} d^{-1}. A second Kelvin wave in late April 1997 resulted in another depression in primary production rate of 33 mmol C m^{-2} d^{-1} at the beginning of May (Chavez et al., 1998). The simulated primary production rates for May 1997 are consistent with these observations (Fig. 3) in that the effect of the downwelling Kelvin wave at the beginning of 1997 is apparent. The simulated distributions show a rapid decrease in primary production during May 1997, which then begins to increase gradually in late June.

The onset of the 1997 El Niño in the simulated distributions is consistent with observations (Fig. 4A–E). However, the maximum in the simulated chlorophyll *a* increase that is associated with the 1998 La Niña occurs during February 1998, which is inconsistent with SeaWiFS-derived chlorophyll *a* concentrations which show that the maximum surface bloom occurs in June–July (Fig. 14A). The reason for this mismatch may be seen in the simulated nutrient fields.

During early 1998, the simulated ammonium and iron concentrations increase in the Cold Tongue (Fig. 7B and C). The increase in iron is due to the combined effects of upwelling and high remineralization rates. Towards the end of the 1997 El Niño, the EUC at 0°N, 140°W starts to shoal which injects nutrient-rich waters into the upper water column. At the same time, the surface waters are warm, which results in high algal growth rates and remineralization rates. Intrusion of nutrients into the euphotic zone initiates a phytoplankton bloom and high remineralization of iron and ammonium strengthens the magnitude of this bloom. During the 1997 El Niño, the water properties in the Cold Tongue are similar to typical Warm Pool conditions Fig. 2A). The surface waters are strongly stratified, with warm waters extending to the bottom of the euphotic zone. Radenac et al. (2001) showed that during this period Warm Pool might have extended to 0°N, 140°W. For such conditions, it is possible that the depths of the isohaline and isothermal layers differed, as happens in the Warm Pool (Lukas and Lindstrom, 1991). Also Vialard and Delecluse (1998) showed that the Barrier Layer displays large interannual migrations and during El Niño phases it moves eastwards and can reach 140°W during mature El Niños. These dynamics are not included in the current model structure. Therefore, this mechanism, which retains high nutrient waters (Mackey et al., 1995; Radenac and Rodier, 1996), could also have been in effect at 0°N, 140°W during the 1997–1998 ENSO conditions. The result is an earlier La Niña increase in the simulated chlorophyll distributions than indicated by the SeaWiFS-derived chlorophyll *a* observations (Fig. 14A). Recently, Ryan et al. (2006) hypothesized that the occurrence of blooms following the El Niño events cannot be explained by local enhancement of vertical nutrient flux, instead the 1998 bloom at 140°W occurs when iron-enriched EUC waters reach the euphotic zone. They argue that the iron-enriched waters only reach the euphotic zone of 140°W towards June 1998 because of changes in the New Guinea Coastal Undercurrent (which is the primary source of iron-enriched waters to the EUC) during El Niño. If their hypothesis is true then the cold EUC waters entering the euphotic zone at the beginning of 1998 can possibly be relatively poor in iron, whereas in the model they introduce iron enriched waters into the euphotic zone resulting in an increase in the chlorophyll *a* concentrations earlier than observed.

The simulated chlorophyll *a* concentrations remain low at 140°W during April–July because anomalously low water temperatures result in low growth rates. The estimated mixed layer depths for April–June are also low (Fig. 2B), which reduces the intrusion of nutrient-rich waters into the surface

Please cite this article as: Salihoglu, B., Modeling the effect of ENSO on the lower trophic level ecosystem of the Cold Tongue and the Warm Pool regions in the equatorial Pacific, Journal of Marine Systems (2009), doi:10.1016/j.jmarsys.2008.12.004

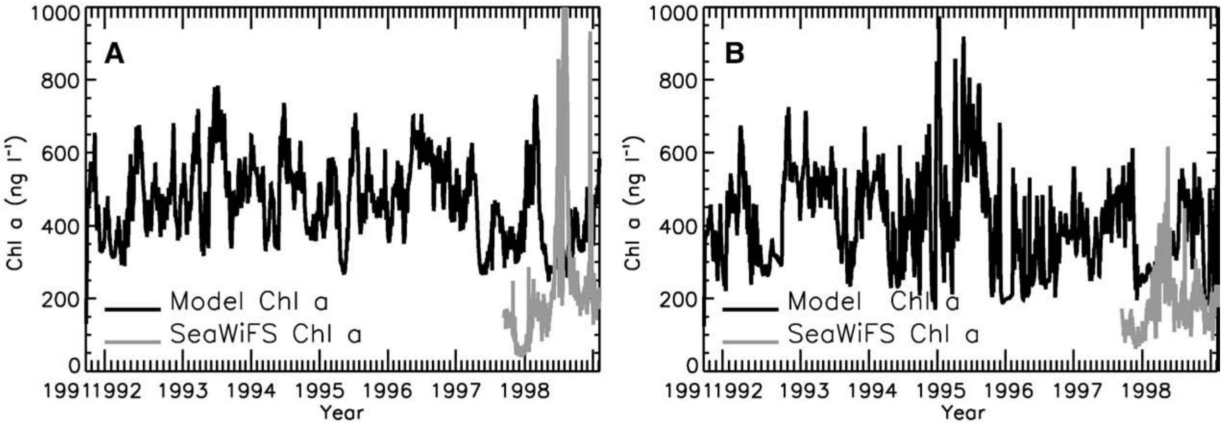

Fig. 14. Comparison of simulated chlorophyll *a* (black) with chlorophyll *a* derived from Sea-viewing Wide Field of view Sensor (SeaWiFS) measurements (grey) at 0°N, 140°W (A) and at 0°N, 165°E (B). The SeaWiFS data set begins in Fall 1997.

waters. Also, Murtugudde et al. (1999) and Picaut et al. (2002) showed that the persistent northerly winds towards the end of 1997–1998 El Niño resulted in a northward shift of the equatorial divergence. The first bloom after the El Niño appeared several degrees to the north of the equator during February 1998 (Murtugudde et al., 1999). This is a relatively weak bloom with chlorophyll concentrations of 0.3 mg m^{-3} and it moved towards the equator during February–June 1998. The unusually strong ($>$1.0 mg m^{-3} chlorophyll *a*) 1998 bloom appeared on the equator in June and persisted until the end of August (Murtugudde et al., 1999). These observations suggest that non-local effects can be an important factor in regulating the chlorophyll biomass on the equator. Part of the mismatch between the observed and modeled chlorophyll *a* during 1998 La Ninã may be due to horizontal advection of phytoplankton into the Cold Tongue region. Thus, non-local factors can contribute to differences in the timing and/or intensity of blooms in the simulated and satellite-derived chlorophyll *a* concentrations. The model structure used in this study does not have the capability of including non-local effects. This highlights the need for development of full three-dimensional models for the equatorial Pacific lower trophic levels.

During the development of the phytoplankton bloom associated with the 1998 La Niña, the mixed layer at 0°N, 140°W deepen, despite a shallow thermocline, resulting in entrainment of nutrients into the surface layer (Murtugudde, personal communication). However, during this period, the mixed layer depths input into the model remain shallow (Fig. 2B) due to the shallow thermocline depths. These results show the importance of and need for inclusion of the range of possible dynamics that effect mixed layer depth (e.g., effect of salinity). The approach used to estimate the mixed layer depths for this study is not sufficiently robust to include all of the relevant dynamics. Future studies should include a mixed layer dynamics that allows for the effects of strong El Niño processes.

The warm phase of the ENSO ends earlier in the Warm Pool compared to the Cold Tongue (Fig. 10A versus 2A). Upwelling of cold waters begins in May 1997 and by January 1998 the cold phase reaches its peak with cold waters extending to the surface (Fig. 10A). For these conditions, the simulated chlorophyll *a* increase that is associated with the 1997 El Niño occurs during June–December 1997. The equivalent increase in the SeaWiFS-derived chlorophyll time series (Fig. 14B) begins in January 1998. The lack of the correct mixed layer dynamics under ENSO conditions in the model in the Warm Pool potentially underlies the mismatch in the simulated and observed chlorophyll blooms.

The effect of temperature on algal growth rates and nutrient remineralization rates can also affect the realism of the Warm Pool simulations. A better representation of temperature effect on algal growth and better information on the remineralization rates of iron and ammonium is needed to increase the model performance for environmental conditions that show extreme variability at short time scales (e.g., ENSO conditions).

6. Conclusions

Simulations show that for the Cold Tongue region, the ENSO warm phase results in a shift to small algal forms (e.g., *Prochlorococcus* spp. and *Synechococcus*) and low primary productivity. In contrast, the phytoplankton community biomass of the Warm Pool is increasingly dominated by larger algal forms (e.g., autotrophic eukaryotes) and primary production is enhanced.

Simulated primary production and carbon export flux in the Cold Tongue are higher than those for the Warm Pool, although the iron levels are much higher in the Warm Pool. This suggests that the higher primary production levels in the Cold Tongue are not due to iron, but rather are a result of the high macronutrient concentrations in the region. Although the simulated primary production is higher in the Cold Tongue compared to the Warm Pool, the phytoplankton growth rates are still well below their physical potentials mainly due to iron control. The combined effects of macronutrients and iron control the Warm Pool primary productivity. Although it is hypothesized that the lower trophic level dynamics in the Warm Pool region is mainly regulated by macronutrients (Le Borgne et al., 2002), the effect of iron regulation on phytoplankton in the region is not known. The effect of nutrient dynamics in regulating the Warm Pool primary productivity is still an area of investigation.

Please cite this article as: Salihoglu, B., Modeling the effect of ENSO on the lower trophic level ecosystem of the Cold Tongue and the Warm Pool regions in the equatorial Pacific, Journal of Marine Systems (2009), doi:10.1016/j.jmarsys.2008.12.004

This study helps to identify important gaps in knowledge of the effect of ENSO processes on the equatorial Pacific ecosystem dynamics. The timing of the observed 1998 blooms was later than what is simulated in the Cold Tongue and the Warm Pool regions. These results suggest either a formation of a high salinity barrier layer structure during this period that delays the intrusion of nutrients or non-local processes can be in play. It is possible that the cold waters intruding the euphotic zone at the beginning of 1998 can be relatively poor in iron or high chlorophyll concentrations observed on the equator can be advected from North, or combination of both can be valid.

Although there are many potential avenues for better representation of the biology in the lower trophic level ecosystem model used in this study, it is the representation of the physical dynamics that provides the primary constraints on the realism of the simulated distributions. In particular the changes in mixed layer dynamics and vertical advection associated with the transition periods from highly stratified conditions to upwelling conditions (ENSO) are not well represented by the approach used to specify the environmental structure. Future studies should include a mixed layer dynamics model that allows for more robust responses in the environment to ENSO conditions. This can be achieved by fully coupling the ecosystem model to a three-dimensional model that includes a realistic mixing scheme (e.g., Chen et al., 1994; Murtugudde et al., 1996), which would resolve high frequency variability resulting from the physical forcing fields (e.g., temperature, mixed layer depth, vertical velocity). Also, the complicated processes involved with the iron transport along the equatorial Pacific Ocean need to be better understood and included in carbon cycle models.

Acknowledgments

This work would not have been possible without the hard work of the TAO Project Office, I would like to thank Dr. Michael McPhaden, Director, for the use of the extensive data available from their mooring array, as well as the SeaWiFS Project and the Distributed Active Archive Center at the Goddard Space Flight Center, for the production and distribution of these data. I wish to thank the programme leader, Dr. Robert Le Borgne for the FLUPAC data, Drs. Martine Rodier for nutrients, Jacques Neveux for photosynthetic pigments, Dr. Aubert Le Bouteiller for ^{14}C uptake measurements. Thanks to the program leader Dr. James Murray for Zonal Flux data, Dr. Martine Rodier for nutrients, Dr. Aubert Le Bouteiller for pigments and primary productivity. Thanks to Dr. Paul Ginoux for his atmospheric dust model output. Constructive conversations with Eileen Hofmann throughout all stages of this work are gratefully acknowledged. Drs. Antonio Busalacchi, James Christian, Marjy Friedrichs, John Klinck, Raghu Murtugudde, Larry Atkinson, Marie-Helene Radenac and Bettina Fach provided helpful comments on earlier presentations of this research. I also thank two anonymous reviewers for constructive comments on an earlier version of the manuscript. This research was generously supported by the National Aeronautics and Space Administration contracts NCC-5-258 and NAG5-11259. The computer facilities and resources were provided by the Commonwealth Center for Coastal Physical Oceanography at Old Dominion University, VA.

References

Alldredge, A.L., Gotschalk, C.C., MacIntyre, S., 1987. Evidence for sustained residence of macrocrustacean fecal pellets in surface waters off Southern California. Deep-Sea Research 34, 1641–1652.

Anis, A., Moum, J.N., 1994. Prescriptions for heat flux and entrainment rates in the upper ocean during convection. Journal of Physical Oceanography 24, 2142–2155.

Archer, D., 1999. Modeling CO_2 in the ocean: a review. In: Bouwman, A.F. (Ed.), Scaling of Trace Gas Fluxes Between Terrestrial and Aquatic Ecosystems and the Atmosphere. Elsevier, Amsterdam.

Aufdenkampe, A.K., Murray, J.W., 2002. Controls on new production: the role of iron and physical processes. Deep-Sea Research II 49, 2649–2668.

Aufdenkampe, A.K., McCarthy, J.J., Rodier, M., Navarette, C., Dunne, J.P., Murray, J.W., 2001. Estimation of new production in the tropical pacific. Global Biogeochemical Cycles 15, 101–113.

Barber, R.T., Chavez, F.P., 1991. Regulation of primary productivity rate in the equatorial Pacific. Limnology and Oceanography 36 (8), 1803–1815.

Barber, R.T., Sanderson, M.P., Lindley, S.T., Chai, F., Newton, J., Trees, C.C., Foley, D.G., Chavez, F.P., 1996. Primary productivity and its regulation in the equatorial Pacific during and following the 1991–1992 El Niño. Deep-Sea Research II 43 (4–6), 933–969.

Behrenfeld, M.J., Bale, A.J., Kolber, Z.S., Aiken, J., Falkowski, P.G., 1996. Confirmation of iron limitation of phytoplankton photosynthesis in the equatorial Pacific Ocean. Nature 383 (6600), 508–511.

Behrenfeld, M.J., Worthington, K., Sherrell, R.M., Chavez, F.P., Strutton, P., McPhaden, M., Shea, D.M., 2006. Controls on tropical pacific ocean productivity revealed through nutrient stress diagnostics. Nature 442, 1025–1028.

Bidigare, R.R., Ondrusek, M.E., 1996. Spatial and temporal variability of phytoplankton pigment distributions in the central equatorial Pacific Ocean. Deep-Sea Research II 43 (4–6), 809–833.

Blanchot, J., Rodier, M., Le Bouteiller, A., 1992. Effect of El Niño Southern Oscillation events on the distribution and abundance of phytoplankton in the western Pacific Tropical Ocean along 165°E. Journal of Plankton Research 14 (1), 137–156.

Chavez, F.P., 1989. Size distribution of phytoplankton in the central and eastern Pacific Ocean. Global Biogeochemical Cycles 3, 27–35.

Chavez, F.P., Buck, K.R., Service, S.K., Newton, J., Barber, R.T., 1996. Phytoplankton variability in the eastern and central Tropical Pacific. Deep-Sea Research II 43, 809–833.

Chavez, F.P., Strutton, P.G., Friedrich, G.E., Feely, R.A., Feldman, G.C., Foley, D.G., McPhaden, M.J., 1999. Biological and chemical response of the equatorial Pacific Ocean to the 1997–98 El Niño. Science 286 (5447), 2126–2131.

Chavez, F.P., Strutton, P.G., McPhaden, M.J., 1998. Biological–physical coupling in the central equatorial Pacific during the onset of the 1997–98 El Niño. Geophysical Research Letters 25 (19), 3543–3546.

Chen, D., Rothstein, L.M., Busalacchi, A.J., 1994. A hybrid vertical mixing scheme and its application to tropical ocean models. Journal of Physical Oceanography 24 (10), 2156–2179.

Christian, J.R., Verschell, M.A., Murtugudde, R., Busalacchi, A.J., McClain, C.R., 2002a. Biogeochemical modelling of the tropical Pacific Ocean. I. Seasonal and interannual variability. Deep-Sea Research II 49, 509–543.

Coale, K.H., Johnson, K.S., Fitzwater, S., Gordon, R., Tanner, S., Chavez, F., Ferioli, L., Sakamoto, C., Rogers, P., Millero, F., Steinberg, P., Nightingale, P., Cooper, D., Cochlan, W.P., R, K., 1996a. A massive phytoplankton bloom induced by an ecosystem-scale iron fertilization experiment in the equatorial Pacific Ocean. Nature 383 (6600), 495–501.

Coale, K.H., Fitzwater, S.E., Gordon, R.M., Johnson, K.S., Barber, R.T., 1996b. Control of community growth and export production by upwelled iron in the equatorial Pacific Ocean. Nature 379 (6566), 621–624.

Conkright, M.E., Garcia, H.E., O'Brien, T.D., Locarnini, R.A., Boyer, T.P., Stephens, C., Antonov, J.I., 2002. World Ocean Atlas 2001, volume 4: Nutrients. S. Levitus. U.S. Government Printing Office, Washington, D.C., NOAA Atlas NESDIS 52 Edition, 392 pp.

Cullen, J.J., Lewis, M.R., Davis, C.O., Barber, R.T., 1992. Photosynthetic characteristics and estimated growth rates indicate grazing is the proximate control of primary production in the equatorial Pacific. Journal of Geophysical Research 97 (C1), 639–654.

Dam, H.G., Zhang, X., Butler, M., Roman, M.R., 1995. Mesozooplankton grazing and metabolism at the equator in the central Pacific: implications for carbon and nitrogen fluxes. Deep-Sea Research II 42 (2–3), 735–756.

D'Asaro, E.A., Farmer, D.M., Osse, J.T., Dairiki, G.T., 1996. A Lagrangian float. Journal of Atmospheric and Oceanic Technology. 13, 130–1246.

Denman, K.L., Marra, J., 1986. Modeling the time dependent photoadaptation to fluctuating light. In: Nihoul, J.C.J. (Ed.), Marine Interface Ecohydrodynamics. Elsevier, Amsterdam, pp. 341–359.

Droop, M.R., 1973. Some thoughts on nutrient limitation in algae. Journal of Phycology 9 (3), 264–272.

Please cite this article as: Salihoglu, B., Modeling the effect of ENSO on the lower trophic level ecosystem of the Cold Tongue and the Warm Pool regions in the equatorial Pacific, Journal of Marine Systems (2009), doi:10.1016/j.jmarsys.2008.12.004

Duce, R.A., Tindale, N.W., 1991. Atmospheric transport of iron and its deposition in the ocean. Limnology and Oceanography 36, 1715–1726.

Duce, R.A., et al., 1991. The atmospheric input of trace species to the world ocean. Global Biogeochemical Cycles 5, 193–259.

Dugdale, R.C., Wilkerson, F.P., 1998. Silicate regulation of new production in the equatorial Pacific upwelling. Nature 391, 270–273.

Dunne, J.P., Murray, J.W., Rodier, M., Hansell, D.A., 2000. Export flux in the western and central equatorial Pacific: zonal and temporal variability. Deep-Sea Research I 47, 901–936.

Firing, E., Lukas, R., Sadler, J., Wyrtki, K., 1983. Equatorial undercurrent disappears during 1982–83 El Niño. Science 222, 1121–1123.

Foley, D.G., Dickey, T.D., McPhaden, M.J., Bidigare, R.R., Lewis, M.R., Barber, R.T., Lindley, S.T., Garside, C., Manov, D.V., McNeil, J.D., 1997. Longwaves and primary productivity variations in the equatorial Pacific at 0°, 140°W. Deep-Sea Research II 44 (9–10), 1801–1826.

Friedrichs, M.A.M., Hofmann, E.E., 2001. Physical control of biological processes in the central equatorial Pacific Ocean. Deep-Sea Research I 48 (4), 1023–1069.

Fung, I.Y., Meyn, S.K., Tegen, I., Doney, S.C., John, J.G., Bishop, J.K.B., 2000. Iron supply and demand in the upper ocean. Global Biogeochemical Cycles 14, 281–295.

Gardner, W.D., Pyo, C.S., Richardson, M.J., Walsh, I.D., 1995. The oceanic mixed-layer pump. Deep-Sea Research II 42, 757–775.

Ginoux, P., Chin, M., Tegen, I., Prospero, J., Holben, B., Dubovik, O., Lin, S.J., 2001. Sources and distributions of dust aerosols simulated with the GOCART model. Journal of Geophysical Research 106, 20225–20273.

Goldman, J.C., 1980. Physiological processes, nutrient availability, and the concept of relative growth rate in marine phytoplankton ecology. In: Falkowski, P.G. (Ed.), Primary Productivity in the Sea. Plenum Press, New York, pp. 179–194.

Goldman, J.C., 1982. Comparative rapid ammonium uptake by four species of marine phytoplankton. Limnology and Oceanography 27 (5), 814–827.

Goldman, J.C., Glibert, P.M., 1983. Inorganic nitrogen uptake by phytoplankton. In: Carpenter, E., Carpone, D.G. (Eds.), Nitrogen in the Marine Environment. Academic Press, New York, pp. 233–274.

Gorgues, T., Menkes, C., Aumont, O., Vialard, J., Dandoneau, Y., Bopp, L., 2005. Biogeochemical impact of tropical instability waves in the equatorial pacific. Geophysical Research Letters 32.

Gregg, W.W., Carder, K.L., 1990. A simple spectral solar irradiance model for cloudless maritime atmospheres. Limnology and Oceanography 35 (8), 1657–1675.

Halpern, D., 1980. A Pacific equatorial temperature section from 172°E to 110°W during Winter and Spring 1979. Deep-Sea Research 27, 931–940.

Hansen, D.V., 1990. Physical aspects of the El Niño event of 1982–1983. In: Glenn, P. (Ed.), Global Ecological Consequences of the 1982–1983 El Niño-Southern Oscillation. Elsevier, Amsterdam, p. 563.

Higgins, H.W., Mackey, D.J., 2000. Algal class abundances, estimated from chlorophyll and carotenoid pigments, in the western equatorial Pacific under El Niño and non-El Niño conditions. Deep-Sea Research I 47 (8), 1461–1483.

Iriarte, J.L., Fryxell, G.A., 1995. Microphytoplankton at the equatorial Pacific (140°W) during the JGOFS EqPac Time Series studies: March to April and October 1992. Deep-Sea Research II 42 (2–3), 559–583.

Ishizaka, J., K, H., Ishikawa, K., Kiyosawa, H., Furusawa, H., Watanabe, Y., Ishida, H., Suzuki, K., Handa, N., Takahashi, M., 1997. Size and taxonomic plankton community structure and carbon flow at the equator of the central Pacific during 1990–1994. Deep-Sea Research II 44, 1927–1949.

Johnson, K.S., Moore, J.K., Smith, W.O., 2002. A report on the U.S. JGOFS workshop on iron dynamics in the carbon cycle. Tech. rep., Moss Landing, California.

Kerr, R.C., Kuiper, G.S., 1997. Particle settling through a diffusive-type thermohaline staircase in the ocean. Deep-Sea Research 44, 399–412.

Landry, M.R., Kirshtein, J., Constantinou, J., 1995. A refined dilution technique for measuring the community grazing impact of microzooplankton, with experimental tests in the central equatorial Pacific. Marine Ecology Progress Series 120 (1–3), 53–63.

Landry, M.R., Kirshtein, J., Constantinou, J., 1996. Abundances and distributions of picoplankton populations in the central equatorial Pacific from 12°N to 12°S, 140°W. Deep-Sea Research II 43 (4–6), 871–890.

Landry, M.R., Barber, R.T., Bidigare, R.R., Chai, F., Coale, K.H., Dam, H.G., Lewis, M.R., Lindley, S.T., McCarthy, J.J., Roman, M.R., Stoecker, D.K., Verity, P.G., White, J.R., 1997. Iron and grazing constraints on primary production in the central equatorial Pacific: An EqPac synthesis. Limnology and Oceanography 42 (3), 405–418.

Landry, M.R., Ondrusek, M.E., Tanner, S.J., Brown, S.L., Constantinou, J., Bidigare, R.R., Coale, K.H., Fitzwater, S., 2000. Biological response to iron fertilization in the eastern equatorial Pacific (IronEx II). 1. Microplankton community abundances and biomass. Marine Ecology Progress Series 201, 17–42.

Latasa, M., Landry, M.R., Schlueter, L., Bidigare, R.R., 1997. Pigment-specific growth and grazing rates of phytoplankton in the central equatorial Pacific. Limnology and Oceanography 42 (2), 289–298.

Laws, E.A., Falkowski, P.G., Smith, W.O., Ducklow, H., McCarthy, J.J., 2000. Temperature effects on export production in the open ocean. Global Biogeochemical Cycles 14, 1231–1246.

Le Borgne, R., Feely, R.A., Mackey, D.J., 2002. Carbon fluxes in the equatorial Pacific: A synthesis of the JGOFS programme. Deep-Sea Research II 49, 2425–2442.

Leonard, C.L., McClain, C.R., Murtugudde, R., Hofmann, E.E., Harding, L.W.J., 1999. An iron-based ecosystem model of the central equatorial Pacific. Journal of Geophysical Research 104 (C1), 1325–1341.

Lindley, S.T., Bidigare, R.R., Barber, R.T., 1995. Phytoplankton photosynthesis parameters along 140°W in the equatorial Pacific. Deep-Sea Research II 42 (2–3), 441–463.

Lukas, R., Lindstrom, E., 1991. The mixed layer of the western equatorial Pacific. Journal of Geophysical Research 96, 3343–3357.

Mackey, D.J., Parslow, J., Higgins, H.W., Griffiths, F.B., O'Sullivan, J.E., 1995. Plankton productivity and biomass in the western equatorial Pacific: Biological and physical controls. Deep-Sea Research II 42 (2–3), 499–533.

Mackey, D.J., Parslow, J.S., Griffiths, F.B., Higgins, H.W., Tilbrook, B., 1997. Phytoplankton productivity and the carbon cycle in the western equatorial Pacific under El Niño and non-El Niño conditions. Deep-Sea Research II 44, 1951–1978.

Martin, J.H., Broenkow, W.W., Fitzwater, S.E., Gordon, R.M., 1990. Yes, it does: A reply to the comment by Banse. Limnology and Oceanography 35 (3), 775–777.

Martin, J.H., Gordon, R.M., Fitzwater, S.E., 1991. The case for iron. Limnology and Oceanography 36 (8), 1793–1802.

Martin, J.H., et al., 1994. Testing the iron hypothesis in ecosystems of the equatorial Pacific Ocean. Nature 371 (6493), 123–129.

McPhaden, M.J., 1999. Genesis and evolution of the 1997–1998 El Niño. Science 283, 950–954.

McPhaden, M.J., Busalacchi, A.J., Cheney, R., Donguy, J.-R., Gage, K.S., Halpern, D., Ji, M., Julian, P., Meyers, G., Mitchum, G.T., Niiler, P.P., Picaut, J., Reynolds, R.W., Smith, N., Takeuchi, K., 1998. The Tropical Ocean-Global Atmosphere observing system: a decade of progress. Journal of Geophysical Research 103 (C7), 14,169–14,240.

Moore, J.K., Doney, S.C., Kleypas, J.A., Glover, D.M., Fung, I.Y., 2002. An intermediate complexity marine ecosystem model for the global domain. Deep-Sea Research II 49, 403–462.

Murray, J.W., Leinen, M.W., Feely, R.A., Toggweiler, J.R., Wanninkhof, R., 1992. EqPac: a process study in the central equatorial Pacific. Oceanography 5, 134–142.

Murray, J.W., Barber, R.T., Roman, M.R., Bacon, M.P., Feely, R.A., 1994. Physical and biological controls on carbon cycling in the equatorial Pacific. Science 266, 58–65.

Murray, J., Johnson, E., Garside, C., 1995. A U.S. JGOFS process study in the equatorial Pacific (EqPac): Introduction. Deep-Sea Research II 42 (2–3), 275–293.

Murtugudde, R., Seager, R., Busalacchi, 1996. Simulation of the tropical oceans with an ocean GCM coupled to an atmospheric mixed-layer model. Journal of Climate 9 (8), 1795–1815.

Murtugudde, R.G., Signorini, S.R., Christian, S.R., Busalacchi, A.J., McClain, C.R., Picaut, J., 1999. Ocean color variability of the tropical Indo-Pacific basin observed by SeaWiFS during 1997–1998. Journal of Geophysical Research 104, 18351–18366.

Nelson, D.M., Treguer, P., Brzezinski, M.A., Leynaert, A., Queaguiner, B., 1995. Production and dissolution of biogenic silica in the ocean: revised global estimates, comparison with regional data and relationship to biogenic sedimentation. Global Biogeochemical Cycles 9, 359–372.

Pacanowski, R.C., Philander, S.G.H., 1981. Parameterization of vertical mixing in numerical models of tropical oceans. Journal of Physical Oceanography 11 (11), 1443–1451.

Philander, G., 1990. El Niño, La Niña, and the Southern Oscillation. Academic Press, Inc., Princeton, New Jersey.

Picaut, J., Hackert, E., Busalacchi, A.J., Murtugudde, R., Lagerloef, G.S.E., 2002. Mechanisms of the 1997–1998 El Niño–La Niña, as inferred from space-based observations. Journal of Geophysical Research 107, 1–20.

Price, F., Weller, R., Pinkel, R., 1986. Diurnal cycling: Observations and models of the upper ocean response to diurnal heating, cooling, and wind mixing. Journal of Geophysical Research 91, 8411–8427.

Price, N.M., Ahner, B.A., Morel, F.M.M., 1994. The equatorial Pacific Ocean: grazer-controlled phytoplankton populations in an iron-limited ecosystem. Limnology and Oceanography 39 (3), 520–534.

Radenac, M.H., Rodier, M., 1996. Nitrate and chlorophyll distributions in relation to thermohaline and current structures in the western tropical Pacific during 1985–1989. Deep-Sea Research II 43 (4–6), 725–752.

Radenac, M., Menkes, C., Vialard, J., Moulin, C., Dandonneau, Y., Delcroix, T., Dupouy, C., Stoens, A., Deschamps, P., 2001. Modeled and observed impacts of the 1997–1998 El Niño on nitrate and new production in the equatorial pacific. Journal of Geophysical Research 106, 26,879.

Rodier, M., Le Borgne, R., 1997. Export flux of particles at the equator in the western and central Pacific Ocean. Deep-Sea Research II 44, 2085–2113.

Please cite this article as: Salihoglu, B., Modeling the effect of ENSO on the lower trophic level ecosystem of the Cold Tongue and the Warm Pool regions in the equatorial Pacific, Journal of Marine Systems (2009), doi:10.1016/j.jmarsys.2008.12.004

Ryan, J.P., Ueki, I., Chao, Y., Zhang, H., Polito, P.S., Chavez, F.P., 2006. Western Pacific modulation of large phytoplankton blooms in the central and eastern equatorial Pacific. Journal of Geophysical Research 111.

Salihoglu, B., 2005. Modeling the effects of physical and biogeochemical processes on phytoplankton species and carbon production in the equatorial Pacific Ocean. Ph.D. thesis, Old Dominion University.

Salihoglu, B., Hofmann, E.E., 2007. Simulations of phytoplankton species and carbon production in the equatorial Pacific Ocean 1. Model configuration and ecosystem dynamics. Journal of Marine Research 65, 219–273.

Schudlich, R.R., Price, J.F., 1992. Diurnal cycles of current, temperature, and turbulent dissipation in a model of the equatorial upper ocean. Journal of Geophysical Research 97, 5409–5422.

Sprintall, J., McPhaden, M.J., 1994. Surface layer variations observed in multiyear time series measurements from the western equatorial Pacific. Journal of Geophysical Research 99, 963–979.

Stoens, A., Menkes, C., Radenac, M., Dandonneau, Y., Nicolas, G., Eldin, G., Laurent, M., Navarette, C., Andre, J.M., Moutin, T., Raimbault, P., 1999. The coupled physical new production system in the equatorial Pacific during the 1992–1995 El Niño. Journal of Geophysical Research 104, 3323–3340.

Strutton, P.G., Chavez, F.P., 2000. Primary productivity in the equatorial Pacific during the 1997–98 El Niño. Journal of Geophysical Research 105, 26,089–26,101.

Tomczak, M., Godfrey, J.S., 1994. Regional Oceanography: An Introduction. Pergamon, New York.

Trenberth, K.E., Hoar, T.J., 1996. The 1990–1995 El Niño-Southern Oscillation event longest on record. Geophysical Research Letters 23, 57–60.

Verity, P.G., Stoecker, D.K., Sieracki, M.E., Nelson, J.R., 1996. Microzooplankton grazing of primary production at 140°W in the equatorial Pacific. Deep-Sea Research II 43 (4–6), 1227–1256.

Vialard, J., Delecluse, P., 1998. An OGCM study for the TOGA decade. part II: Barrier Layer formation and variability. Journal of Physical Oceanography 28, 1089–1106.

Walsh, J.J., 1976. Herbivory as a factor in patterns of nutrient utilization in the sea. Limnology and Oceanography 21, 1–13.

Wyrtki, K., 1975. El Niño – the dynamic response of the equatorial Pacific Ocean to atmospheric forcing. Journal of Physical Oceanography 5, 572–584.

Wyrtki, K., 1985. Water displacements in the Pacific and the genesis of El Niño cycles. Journal of Geophysical Research 90, 7129–7132.

Yu, X., McPhaden, J.M., 1999. Seasonal variability in the equatorial Pacific. Journal of Physical Oceanography 29, 925–947.

Zhang, X., Dam, H.G., White, J.R., Roman, M.R., 1995. Latitudinal variations in mesozooplankton grazing and metabolism in the central tropical Pacific during the U.S. JGOFS EqPac study. Deep-Sea Research II 42 (2–3), 695–714.

Please cite this article as: Salihoglu, B., Modeling the effect of ENSO on the lower trophic level ecosystem of the Cold Tongue and the Warm Pool regions in the equatorial Pacific, Journal of Marine Systems (2009), doi:10.1016/j.jmarsys.2008.12.004